Escola Politécnica da Universidade de São Paulo
Departamento de Engenharia Química
PQI 2409 Laboratório de Operações Unitárias e Reatores

Experiência
DESSORÇÃO DE AMÔNIA

OBJETIVOS

Estudo hidrodinâmico de uma coluna de enchimento. Determinação da altura da unidade de transferência de massa global para a dessorção de amônia. Determinação da altura equivalente a um estágio teórico para a dessorção de amônia.

EQUIPAMENTO

A coluna , cujo esquema é mostrado na figura 1, tem diâmetro de 3" e altura de 1,5 m, sendo recheada de anéis de Raschig de vidro de 3/8".

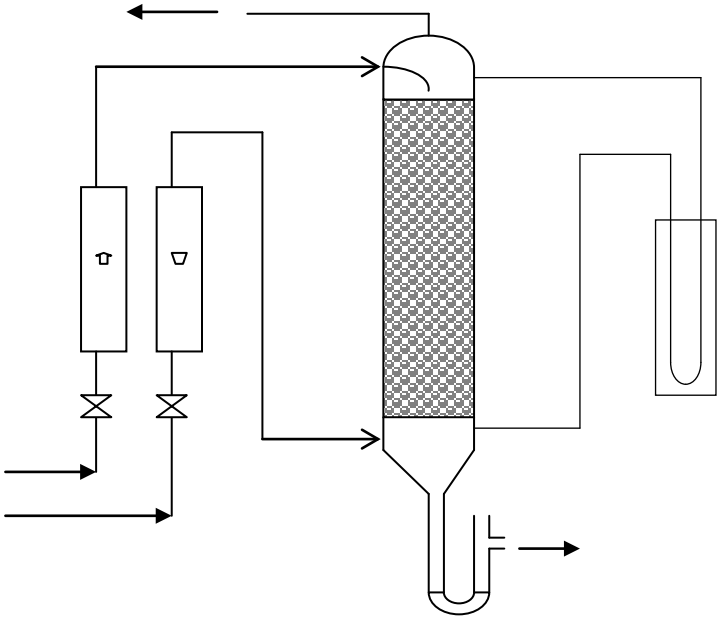

Figura 1. Esquema do equipamento experimental.

PROCEDIMENTO EXPERIMENTAL

Estudo hidrodinâmico

Os fluidos usados são água e ar.

(1) Mantendo a vazão de líquido nula (L=0) e variando a vazão de gás (G), medir a perda de carga (ΔP).
(2) Mantendo a vazão de líquido constante ($L=L_1$ e depois $L=L_2$) e variando a vazão de gás, medir a perda de carga.
(3) Mantendo constante a vazão de gás ($G=G_1$) e variando a vazão de líquido, medir a perda de carga.
(4) Mantendo a perda de carga constante ($\Delta P=\Delta P_1$) e variando as vazões de líquido e de gás, obter a curva característica do sistema.

Estudo do transporte de massa

Os fluidos usados são ar e solução aquosa de amônia. Mantendo as vazões de líquido e de gás constantes ($L=L_3$ e $G=G_3$), obter a perda de carga e medir a concentração da solução de amônia na entrada e na saída da coluna, operando em regime permanente. Anotar os seguintes dados: temperatura e pressão do gás, temperatura da solução na entrada e na saída da coluna, características da coluna (diâmetro da coluna,

tipo, tamanho e material de construção do enchimento, altura do enchimento na coluna), concentração e fator de correção da solução de ácido clorídrico usada nas titulações, volume da amostra retirada da coluna e volume de ácido gasto na titulação.

RELATÓRIO

Generalidades

Apresentar em tabelas, de modo ordenado, todos os dados coletados na experiência e eventuais dados extraídos da literatura, necessários à elaboração do relatório.

(a) Apresentar, em tabelas e gráficos, de modo ordenado, todos os resultados solicitados.
(b) Comentar e analisar os resultados e, sempre que possível, comparar os valores experimentais com os preditos pela literatura.
(c) Apresentar num memorial de cálculos à parte, o desenvolvimento detalhado do tratamento de dados. Devem constar as equações usadas, os valores das variáveis, as hipóteses simplificadoras, os cálculos pormenorizados, as fontes bibliográficas das informações extraídas, etc.
(d) Apresentar numa relação anexa, a nomenclatura das variáveis e a respectiva unidade adotada.

Estudo hidrodinâmico

(1) Corrigir as vazões lidas nos rotâmetros (ver referência 2).
(2) Construir o gráfico de log ($\Delta P/Z$) versus log G para L=0, L=L_1 e L=L_2, onde Z é a altura do enchimento. No mesmo gráfico, apresentar a correspondente curva prevista pela correlação de Robbins (ref. 3). Use símbolos isolados para os pontos experimentais e linha contínua (cheia e tracejada) para as previsões dos correlações. Compare também os resultados experimentais com a correlação de Engel et a. (ref. 5).
(3) Construir o gráfico de log ($\Delta P/Z$) versus log L para G=G_1. Comparar com as equaçôes de Robbins e de Engel et al..
(4) Construir a curva característica do sistema para $\Delta P=\Delta P_1$. Comparar com o gráfico de Sherwood-Eckert.
(5) É possível caracterizar os pontos de "loading"e de afogamento nesta experiência? Comentar.
(6) Calcular para um dos pontos ensaiados a perda de carga pelo gráfico de Sherwood-Eckert e pela correlação de Robbins (referência 3). Comparar os resultados com o valor experimental
(7) Calcular, para o mesmo ponto do item (6), o fator de afogamento pelo gráfico de Sherwwod-Eckert e pela correlação de Kister-Gill (veja na referência 4). E pela correlação de Engel et al. (ref. 5)
(8) Calcular a altura mínima do selo hidráulico no fundo da coluna.

Estudo do transporte de massa

(1) Calcular a concentração de saída da fase gasosa.
(2) Calcular a altura da unidade de transferência de massa global com base na fase gasosa. Comparar o resultado com o obtido através de correlações da literatura (procurar e reportar).
(3) Calcular a altura equivalente a um estágio teórico.

REFERÊNCIAS BIBLIOGRÁFICAS

[1] C.O. BENNET & J.E. MYERS, *Fenômenos de Transporte* (tradução da 2ª edição de Momentum, Heat and Mass Transfer, 1974), McGraw-Hill, São Paulo, 1978.

[2] W.G.VAUX, Calculating flow through gas rotameters, *Chem. Engng*., December 1, 1980, p. 119-120.

[3] ROBBINS, L.A. Improve pressure-drop prediction with a new correlation. *Chem. Engng. Progr.* V. 87, n. 5, p. 87-91, 1991

[4] KISTER, H.Z.; GILL, D.R. Predict flood point and pressure drop for modern random packings. *Chem. Engng. Progr.*, v. 87, n. 2, p. 32-42, 1991

[5] ENGEL, V.; STICHLMAIR, J.;. GEIPEL, W. Fluid Dynamics of packings for gas-liquid contactors", Chem. Eng. Technol., 24, p.459-462, 2001

Calculating flow through gas rotameters

When you use a rotameter for a gas or condition different from the one it was calibrated for, the readings must be corrected. Here are the formulas that you will need.

Walter Gregson Vaux, Westinghouse R&D Center

☐ If you have a rotameter or other gas flowmeter calibrated for a certain gas, how do you figure settings for other gases, different pressures and temperatures? There is no need to experimentally recalibrate the rotameter for the new conditions. Only a simple formula is needed.

In this article, there is a brief derivation of the formula, and examples to help you calibrate your rotameter and use it for any gas and process conditions.

A rotameter is a gas flowmeter consisting of a metering float in a tapered glass tube. Upwardly flowing gas suspends the float in the tube (Fig. 1). When the gas flowrate increases, the float rises in the tapered tube to provide a larger flow area around the float.

We can view the annular space between the float or ball and rotameter tube as an orifice (see inset in Fig. 2) and apply the orifice equation for gases [*1*]:

$$Q_1\sqrt{\rho_1} = CYS\sqrt{\frac{2g_c\Delta P}{1-\beta^4}} \qquad (1)$$

For a given value of the float position, Z, the discharge coefficient, C, the expansion factor, Y, orifice area, S, Newton's law factor, g_c, cross-section ratio, β, and gas pressure drop, ΔP, across the float are all constant. We can then write:

$$Q_1\sqrt{\rho_1}|_{z=\text{constant}} = \text{constant} \qquad (2)$$

Another way of deriving Eq. (2) is from the Fischer & Porter Co.'s data interpreted by McCabe and Smith [*2*]: For a given rotameter float setting, the value of Eq. (3)—following—is nearly constant:

$$\frac{\rho Q}{D_f\sqrt{m_f g\rho(1-\rho/\rho_f)}} \qquad (3)$$

where Q = volumetric flowrate of gas; D_f = float diameter (Fig. 1); m_f = float mass; g = gravity acceleration; ρ = gas density; ρ_f = float density; μ = gas viscosity.

For a given rotameter float, mass, m_f, and density, ρ_f, are constant. The gas density is much less than the float density, so that $(1-\rho/\rho_f) \approx 1$, whereby:

$$Q_1\sqrt{\rho_1}|_{z=\text{constant}} = \text{constant} \qquad (2)$$

$$Q_1\sqrt{\rho_1} = Q_0\sqrt{\rho_0} \qquad (4)$$

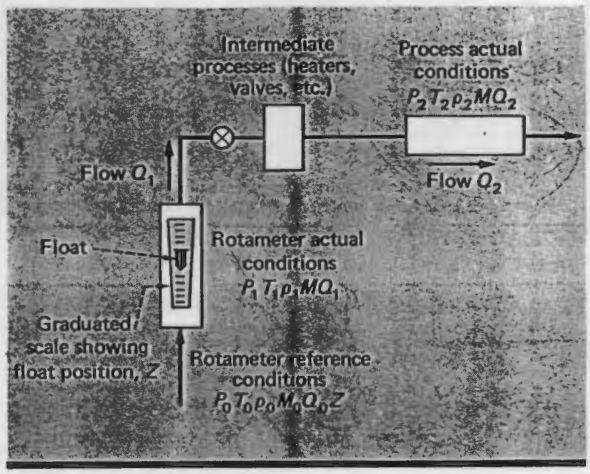

Description of variables for a gas flow system **Fig. 1**

The mass flowrate of gas, ρQ, is constant through a system (such as that pictured in Fig. 1), so that for two points in a system:

$$\rho_1 Q_1 = \rho_2 Q_2 \qquad (5)$$

By the perfect-gas law:

$$\rho = PM/RT \qquad (6)$$

where P = gas pressure; M = gas molecular weight; R = gas constant; T = absolute temperature.

Combining Eq. (4), (5) and (6) gives the working relationships:

For finding the gas flowrate in the process from the rotameter scale reading, Q_0

$$Q_2 = Q_0\frac{T_2}{P_2}\sqrt{\frac{P_0P_1M_0}{T_0T_1M}} \qquad (7)$$

For setting the gas flowrate at the rotameter to give a desired gas flowrate in the process.

$$Q_0 = Q_2\frac{P_2}{T_2}\sqrt{\frac{T_0T_1M}{P_0P_1M_0}} \qquad (8)$$

Often these formulas can be simplified: if the gas temperature in the rotameter equals the rotameter calibration temperature, then $T_0 = T_1$; if the process gas is the same gas used for rotameter calibration, $M = M_0$.

Rotameter calibration

Rotameters are usually calibrated against a wet test meter or another calibrated rotameter. The rotameter

29

Form for rotameter calibration, with example values

Rotameter calibration — *Reference gas: Air, $M_0 = 29$

Wet test meter				Reference conditions			Rotameter conditions					
Q_2 Actual flowrate, cm^3/s	T_2 Actual temperature °C	T_2 K	P_2 *Actual pressure of dry gas, kPa	T_0 K	P_0 kPa	M_0 g/mole	T_1 °C	T_1 K	P_1 kPa	M g/mole	Q_0† from Eq. (7), cm^3/s	Z†
170	25	298	101	293	101	29	27	300	103	29	167	5
300	25	298	101	293	101	29	27	300	103	29	296	10
500	25	298	101	293	101	29	26	299	104	29	489	12
800	24	297	102	293	101	29	26	299	105	29	790	26
1,200	23	296	102	293	101	29	25	298	106	29	1,181	33
1,700	22	295	103	293	101	29	24	297	108	29	1,671	45

*Corrected for water vapor pressure.
†These data fit the calibration curve, $Q_0 = 31.4\,Z^{1.031}$, and are plotted in Fig. 2.

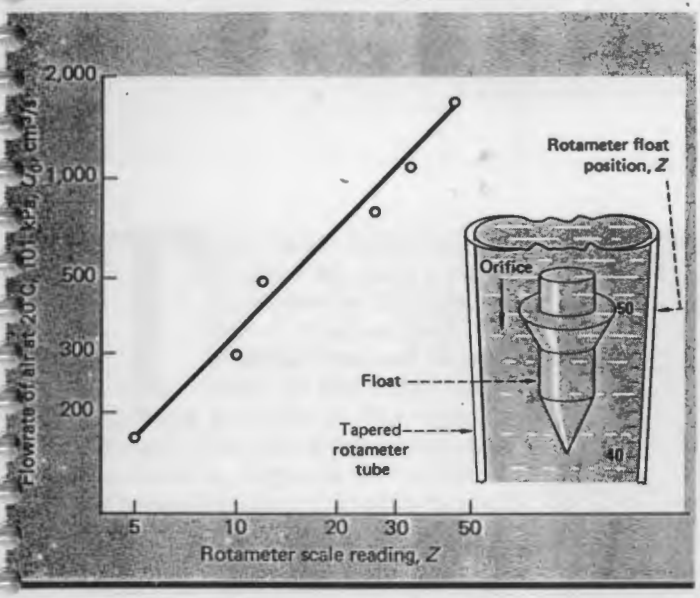

Rotameter calibration curve from data in the Table Fig. 2

being tested will be graduated with arbitrary or approximate flowrate markings. Rotameter readings on the graduated scale are denoted by the symbol Z (Fig. 2).

We need to choose a reference temperature, T_0, pressure, P_0, and gas. Using Eq. (7), we can construct a curve of Q_0 versus Z from calibration measurements, using the form shown in the table.

Usually, rotameter data fit a power curve (log-log) plot closely. The data in the table fit the curve $Q_0 = 31.4\,Z^{1.031}$ (or $Z = 0.0353\,Q_0^{0.970}$) adequately ($r = 0.990$) (Fig. 2).

Setting rotameter for process conditions

For example, consider a fluidized-bed reactor operating at 815°C (1,088 K) and 4 psig (129 kPa). We want a velocity of 2 ft/s (60 cm/s) using carbon dioxide ($M = 44$), rather than the reference gas, air ($M = 29$). With the reactor's cross-sectional area of 60 cm^2, we require:

$$Q_2 = 5{,}400\ cm^3/s$$
$$T_2 = 1{,}088\ K$$
$$P_2 = 129\ kPa$$
$$M = 44$$

The conditions at the rotameter are:

$$T_1 = 11°C\ (262\ K)$$
$$P_1 = 210\ kPa\ (15.8\ psig)$$
$$M = 44$$

The reference conditions for the rotameter are:

$$T_0 = 20°C\ (293\ K)$$
$$P_0 = 101.3\ kPa\ (1\ atm)$$
$$M_0 = 29\ (air)$$

We find the reference flowrate at the rotameter from Eq. (7):

$$Q_0 = Q_2 \frac{P_2}{T_2}\sqrt{\frac{T_0 T_1 M}{P_0 P_1 M_0}}$$
$$= 5{,}400\,\frac{129}{1{,}088}\sqrt{\frac{(293)(262)(44)}{(101.3)(210)(29)}}$$
$$= 1{,}498\ cm^3/s.$$

Using the rotameter calibration formula as the calibration curve (Fig. 2):

$$Z = 0.0353\,Q_0^{0.970}$$
$$= 0.0353(1{,}498)^{0.970}$$
$$= 42$$

Roy V. Hughson, Editor

References

1. Perry, J. H., "Chemical Engineers' Handbook," 3rd ed., McGraw-Hill, New York, 1950, p. 403.
2. McCabe, W. L., and Smith, J. C., "Unit Operations of Chemical Engineering," McGraw-Hill, New York, 1956, p. 122.

The author

Walter Gregson Vaux is a senior engineer at Westinghouse R&D Center, 1310 Beulah Rd., Pittsburgh, PA 15235, where he has been involved in environmental studies and work on fluidized-bed combustion. He holds three degrees in chemical engineering: a B.S. from the University of Washington and an M.S. and Ph.D. from the University of Minnesota. He is a member of AIChE and a registered professional engineer in Pennsylvania.

Circle 418 on Reader Service Card

CHEMICAL ENGINEERING DECEMBER 1, 1980

30

Communications

Fluid Dynamics of Packings for Gas-Liquid Contactors

By *Volker Engel, Johann Stichlmair*, and *Werner Geipel**

1 Introduction

Random and structured packings are beside the trays the commonly used equipment for thermal separation columns. They are used in the field of distillation, scrubbing and stripping. The development of industrial random packings started with the patent of the Raschig ring in 1904. After almost a century development of new types and structures and after the same period of development of models it is still difficult to predict the fluid dynamics and the mass transfer efficiency of packed columns.

At the present state of the art, only empirical models are available. Therefore, it is risky to use these models beyond the range of their validation. Only a few models published in recent years are based on a model structure (e.g., tube model, particle model) and are expected to be applicable to all types and sizes of packings as well as a wide range of physical properties of liquid and gas. Unfortunately, most of these models still need empirical packing parameters.

In this article a new model for the prediction of the liquid holdup, the pressure drop and the flooding of a structured or randomly packed column is presented. The new model only needs the knowledge of the dry pressure drop (as a function of the gas load) and the geometric parameters "void fraction" and "geometric surface array".

2 Fluid Dynamics

The countercurrent flow of gas and liquid in a packed column is characterized by two operating points: loading and flooding. By increasing the liquid flow rate the liquid holdup grows steadily. After reaching the loading point, the holdup increases significantly and reaches its maximum at the flooding point. At this point the countercurrent flow of gas and liquid breaks down.

2.1 Liquid Holdup

The liquid holdup in an irrigated packed column consists of two parts: the static and the dynamic holdup[1]:

$$h_{tot} = h_{stat} + h_{dyn} \tag{1}$$

2.1.1 Static Liquid Holdup

The static holdup is bound by capillary and adhesion forces and remains in the packing after irrigation is stopped. The static liquid holdup is a function of the type, size and material of the packing as well as of the physical properties of the liquid.

Only a few models describing the static holdup are published. Regressing all available experimental data leads to a new correlation incorporating the models of Gelbe [1] and Blass and Kurtz [2]:

$$h_{stat} = 0.033 \cdot \exp\left(-0.22 \frac{g \cdot \rho_L}{\sigma_L \cdot a_{geo}^2}\right) \tag{2}$$

The relative mean deviation of the model to experimental data (100 data points) is about 14 %.

2.1.2 Dynamic Liquid Holdup

There are many published models for the prediction of the liquid holdup in packed columns, but only a few of them do not need empirical parameters.

The complexity of flow conditions makes it almost impossible to describe the detailed mechanism of liquid holdup. The literature shows that incommensurate results are obtained from models addressing only single phenomena of the liquid holdup in random and structured packings. Therefore, this work attempts to express the liquid holdup by correlating relevant dimensionless parameters.

A dimensional matrix of the total liquid holdup can be formed based on the list of relevant factors. This relevance list for the total liquid holdup below the loading point (no influence of the gas flow) comprises the physical properties of the liquid flow (density ρ_L, dynamic viscosity η_L, and surface tension σ_L), the characteristic packing properties (void fraction ε, and specific packing surface a_{geo}), the liquid load u_L, and the acceleration of gravity g.

By matrix transformations (Stichlmair [3]), a complete set of dimensionless numbers can be derived:

[*] Dr.-Ing. V. Engel, WelChem GmbH, Boltzmannstr. 15, D-85748 Garching; Prof. Dr.-Ing. J. Stichlmair, Lehrstuhl für Fluidverfahrenstechnik, TU München, D-85748 Garching; Dr.-Ing. W. Geipel, Rauschert Verfahrenstechnik GmbH, D-96347 Steinwiesen, Germany.

1) List of symbols at the end of the paper.

 © WILEY-VCH Verlag GmbH, D-69469 Weinheim, 2001 0930-7516/01/0505-0459 $ 17.50+.50/0

50

- $\pi_u = \frac{u_L^2 \cdot a_{geo}}{g}$ (Froude number) describes the liquid load.
- $\pi_\eta = \frac{\eta_L^2 \cdot a_{geo}^3}{\rho_L^2 \cdot g}$ (Galileo number) characterizes the flow condition of a liquid film.
- $\pi_\sigma = \frac{\sigma \cdot a_{geo}^2}{\rho_L \cdot g}$ (Bond number) characterizes the wetting and draining behavior.
- $\pi = \varepsilon$ The void fraction ε of the packing is a dimensionless quantity.

Assuming that the holdup can be correlated by a power product of these dimensional numbers, the following applies:

$$h_{dyn0} = C_1 \cdot \pi_u^{C_2} \cdot \pi_\eta^{C_3} \cdot \pi_\sigma^{C_4} \cdot \varepsilon^{C_5} \quad (3)$$

The constants C_1 to C_5 are determined by regression analysis from the data of the data base. The resulting constants are shown in Eq. (4). It shows that the effect of the void fraction ε is negligible. This can be explained by the observation that the liquid is flowing on the surface of the packing and is not effected by the amount of the packing material. If the void fraction ε (or the packing material 1–ε) would have an influence, the liquid holdup of a structured packing with different plate thickness would have to be different.

The correlation is:

$$h_{dyn0} = 3.6 \cdot \left(\frac{u_L \cdot a_{geo}^{1/2}}{g^{1/2}}\right)^{0.66} \left(\frac{\eta_L \cdot a_{geo}^{3/2}}{\rho_L \cdot g^{1/2}}\right)^{0.25} \left(\frac{\sigma \cdot a_{geo}^2}{\rho_L \cdot g}\right)^{0.1} \quad (4)$$

The quality of the correlation is shown in the parity plot in Fig. 1. The mean relative deviation is about 15 %. About 91 % of the data are within the 30 % band.

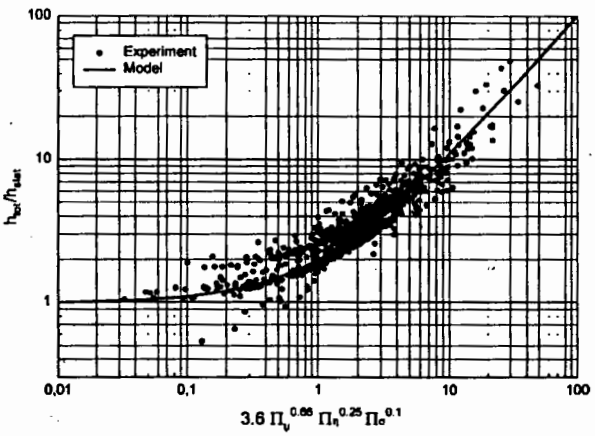

Figure 1. Model of the total liquid holdup without countercurrent flow of gas.

Above the loading point, the liquid holdup increases considerably with increasing liquid load. The loading is also shown in the increasing pressure drop. The coupling of these two effects is described by Stichlmair *et al.* [5]. Here, it is transferred to the dynamic liquid holdup:

$$h_{dyn} = h_{dyn0}\left[1 + 36\left(\frac{\Delta p_{tot}/L}{\rho_L g}\right)^2\right] \quad (5)$$

2.2 Dry Pressure Drop

The complexity of a random packing cannot be described exactly. To reproduce such a complex reality, a model structure is necessary. The model structure has to be as "real" as necessary (to take the main effects into account), but at the same time as "simple" as possible (to achieve a practical correlation).

In literature, different model structures for random and structured packed columns are described. The publication of Stichlmair *et al.* [5] shows the advantages of the particle model. In this model structure, the real packing is replaced by a system of spherical particles which have the same surface and void fraction as the original packing. With these equivalence conditions, the equivalent diameter of the particle d_p is (Eq. (6)):

$$d_p = 6\frac{1-\varepsilon}{a_{geo}} \quad (6)$$

Thus, the originally random structure of the packing is made accessible to calculation. Stichlmair *et al.* [5] show that the correlations for fluidized beds can also be applied to a system of fixed particles. Eq. (7) describes the basic equation of the particle model. The friction factor ψ is derived from the dry pressure drop of the original packing. Therefore, it is one of the characteristic parameters of a random and structured packing, together with the geometric surface a_{geo} and the void fraction ε.

$$\frac{\Delta p_{dry}}{L} = \frac{1}{8}\psi a_{geo}\frac{\rho_G u_G^2}{\varepsilon^{4.65}} \quad (7)$$

In the technical important region, the dry pressure drop can be described with a two-parameter equation, according to the straight line in the logarithmic plot of dry pressure drop vs. gas load.

$$\frac{\Delta p_{tr}}{L} = 10^b F^a \quad (8)$$

The parameters a and b can be easily derived from experimental data. An extensive list (pressure drop parameters, geometric surface and void fraction) of random and structured packings is published in Engel [4].

2.3 Wet Pressure Drop

For the description of the wet pressure drop, the model structure of the "packing particles" and the description of the liquid holdup have to be combined. By analogy with the description of the real packing with the particle model, the liquid holdup should also be described by fluid particles in the model structure (see Fig. 2).

 © WILEY-VCH Verlag GmbH, D-69469 Weinheim, 2001

51

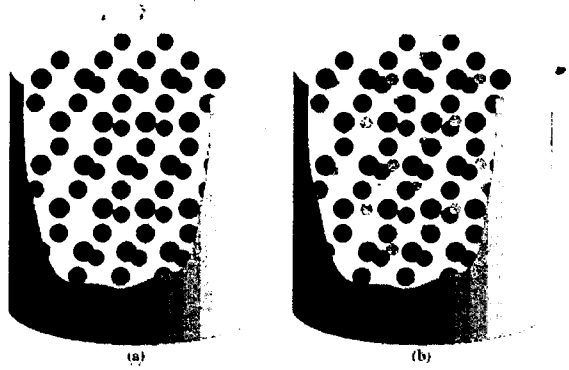

Figure 2. Dry model structure (a) and model structure with liquid holdup (b).

For this derivation, volume, diameter and friction factor of the fluid particles have to be determined. The volume of the fluid particles can be calculated from the knowledge of the liquid holdup (Eq. (5)). For the diameter of the fluid particle, however, a correlation is still missing. A structure for this correlation can be derived from the balance of forces of a falling droplet. Eq. (9) shows the general form of this correlation for the diameter of the fluid particle d_L.

$$d_L = C_L \sqrt{\frac{6\sigma_L}{\Delta\rho g}} \tag{9}$$

The analysis of the experimental data shows that random packings can be calculated with $C_L = 0{,}4$, structured packings with $C_L = 0{,}8$. This difference can be explained with the different flow regimes in random packings (droplet and streams) and in structured packings (film flow).

The last parameter, the friction factor of the fluid particle, equals in a first approximation the friction factor of the dry particle. This approximation is based on the assumption that the liquid film does not change the shape of the packing.

These assumptions result in the following basic equations for wet pressure drop:

$$\Delta p_{tot} = \frac{1}{8}\psi\left(\frac{6h_{dyn}}{d_L} + a_{geo}\right)\frac{\rho_G u_G^2}{\left(\varepsilon - h_{dyn}\right)^{4.65}} \tag{10}$$

To eliminate the friction factor, Eq. (10) can be related to the dry pressure drop:

$$\frac{\Delta p_{tot}}{\Delta p_{dry}} = \frac{\dfrac{6h_{dyn}}{d_L} + a_{geo}}{a_{geo}}\left(\frac{\varepsilon}{\varepsilon - h_{dyn}}\right)^{4.65} \tag{11}$$

As the liquid holdup is a function of the pressure drop, Eq. (11) has to be solved by iteration.

2.4 Operating Point, Flooding Factor

The effectiveness of the presented correlation for the pressure drop can be proven in predicting the operating limits of a column. By inserting the model equations in the mathematical expression for flooding (see [5])

$$\left.\frac{\delta\Delta p_{tot}}{\delta\Delta p_{dry}}\right|_{fl} = \infty \quad \text{or} \quad \left.\frac{\delta\Delta p_{tot}}{\delta\Delta p_{dry}}\right|_{fl} = 0 \tag{12}$$

A correlation for the pressure drop at the flooding point for certain liquid load is found. Eq. (13) is the exact solution (root) of Eq. (12). It can be solved without any iteration.

$$\frac{\Delta p_{tot,fl}}{\rho_L g} = \frac{1}{2988h_{dyn0}}\left(249h_{dyn0}\left(X^{0.5} - 60\varepsilon - 558h_{dyn0} - 103d_L a_{geo}\right)\right)^{0.5} \tag{13}$$

with

$$X = 3600\varepsilon + 186480h_{dyn0}\varepsilon + 32280d_L a_{geo}\varepsilon + 191844h_{dyn0}^2 + 95028d_L a_{geo} h_{dyn0} + 10609d_L^2 a_{geo}^2 \tag{14}$$

The dynamic liquid holdup at the flooding point $h_{dyn,fl}$ (Eq. (15)) and the (fictive) dry pressure drop at the flooding point (Eq.(16)) can be calculated with the pressure drop at the flooding point.

$$h_{dyn,fl} = h_{dyn0}\left[1 + \left(6\frac{\Delta p_{tot,fl}}{\rho_L g}\right)^2\right] \tag{15}$$

$$\Delta p_{dry,fl} = \Delta p_{tot,Fl}\frac{a_{geo}}{\dfrac{6h_{dyn,fl}}{d_L} + a_{geo}}\left(1 - \frac{h_{dyn,fl}}{\varepsilon}\right)^{4.65} \tag{16}$$

For a turbulent flow regime, which is the normal condition in random and structured packings, the flooding factor can be described by Eq. (17). The flooding factor describes the distance to the operation limit for flooding at a certain liquid holdup.

$$\text{Flooding factor} = \sqrt{\frac{\Delta p_{dry}}{\Delta p_{dry,fl}}} \tag{17}$$

3 Conclusion

With this paper, a novel, general model for the description of the fluid dynamics in random and structured packings has been developed. To apply this model, only the geometric surface a_{geo}, the void fraction ε and the dry pressure drop Δp_{dry} of the packing have to be known.

The model makes good predictions for the pressure drop and for the operating condition (flooding factor). In Fig. 3, a comparison of the model and of experimental data from a modern ceramic random packing is shown.

The comparison with a large database of pressure drop measurement (3365 data points) which contains a large number of physical and operating data as well as many different geometries of random and structured packings results in a mean relative deviation of 21 %. The largest

 © WILEY-VCH Verlag GmbH, D-69469 Weinheim, 2001

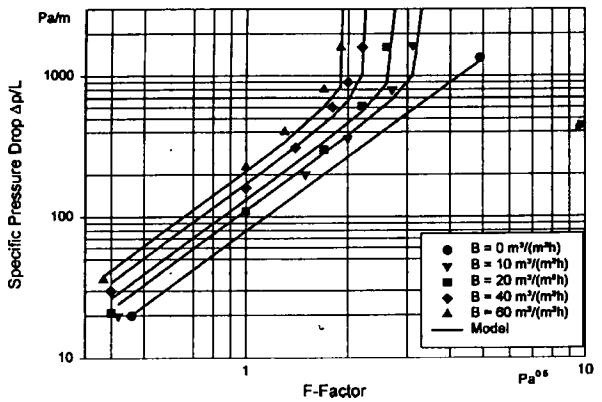

Figure 3. Comparison experiment/model (random packing Hiflow ring 35 mm, type 35–5, ceramics, air/water).

deviations occur at the flooding point. Nevertheless, the gas velocity at the flooding point is very well represented.

Received: December 22, 2000 [K 2664]

Symbols used

a	[m^2/m^3]	specific surface
B	[$m^3/(m^2h)$]	irrigation rate
a,b,C	[–]	constants
d	[m]	diameter
F	[–]	F-factor $F \equiv u_G\sqrt{\rho_G}$
g	[m/s^3]	gravitation
h	[m^3/m^3]	liquid holdup
Δp	[Pa/m]	specific pressure drop
u	[m/s]	superficial velocity
X	[–]	function

Greek symbols

ε	[m^3/m^3]	void fraction
Δ	[–]	difference
μ	[kg/(ms)]	dynamic viscosity
ρ	[kg/m^3]	density
σ	[N/m]	surface tension
ψ	[–]	friction factor
Π	[–]	dimensionless property

Sub- and Superscripts

0	without gas countercurrent, underneath the loading point
dyn	dynamic part
fl	at the flooding point
G	gas
geo	geometric
tot	total
stat	static
L	liquid
P	particle
dry	dry

References

[1] Gelbe, H., A New Correlation for Liquid Holdup in Packed Beds, *Chem. Eng. Sci. 23* (1968) pp. 1401–1403.

[2] BLAß, E.; Kurtz, R., Der Einfluss grenzflächenenergetischer Größen auf den Zweiphasen-Gegenstrom durch Raschigring-Füllkörpersäulen, Teil 1: Flüssigkeitsinhalt, *Verfahrenstechnik 10* (1976) pp. 721.

[3] Stichlmair, J., *Kennzahlen und Ähnlichkeitsgesetze im Ingenieurwesen*, Altos-Verlag, Essen 1990.

[4] Engel, V., Fluiddynamik in Packungskolonnen für Gas/Flüssig-Systeme, *Fortschr.-Ber. VDI*, vol. 605, ser. 3, VDI-Verlag, Düsseldorf 1999.

[5] Stichlmair, J.; Bravo, J. L.; Fair, J. R., General Model for Prediction of Pressure Drop and Capacity of Countercurrent Gas/Liquid Packed Columns, *Gas Sep. & Purif. 3* (1989) pp. 19–28.

This paper was also published in German in Chem. Ing. Tech. 72 (2000) No. 7, pp. 700–703.

Thermal Stability Assessment of Self-Accelerating Decomposition Reactions in the Condensed Phase*

By *Rainer Göllnitz* and *Bernd Reimer*[**]

1 Introduction

Runaway and decomposition reactions in condensed phases contribute considerably to incidents in chemical plants. Frequently, such reactions are the result of unexpected processes, which start with a moderate reaction rate then, due to thermal or autocatalytic effects the reaction is accelerated and may cause an explosion. The pressure effects connected with such explosions are essentially higher than those of fuel-air-explosions. Moreover, hazards arise from the products, which are emitted into the environment after the pressure relief devices have been activated.

Such explosions may occur especially frequently in:

- dryers and distillation equipment,
- batch reactors and
- storage tanks with heating devices.

To illustrate this problem, area-temperature-time data for the decomposition of 2-nitrobenzaldehyde are shown in Fig. 1. The curves were calculated for adiabatic conditions using the kinetic data of Grewer [1]. The specification of an ignition temperature is not sufficient to describe such a reaction, in contrast to explosions of gases and dust in air. In addition to

[*] Paper presented at the DECHEMA joint meeting, 27-29. April 1999 in Wiesbaden.

[**] R. Göllnitz, B. Reimer, Martin-Luther-Universität Halle-Wittenberg, Fachbereich Ingenieurwissenschaften, Institut für Umwelttechnik, D-06099 Halle/Saale.

 © WILEY-VCH Verlag GmbH, D-69469 Weinheim, 2001 0930-7516/01/0505-0462 $ 17.50+.50/0

Predict Flood Point and Pressure Drop for Modern Random Packings

This new procedure, based on a well-established correlation, provides a reliable method for calculating these values.

HENRY Z. KISTER, BROWN & ROOT BRAUN, INC., AND
DAVID R. GILL, SIMULATION SCIENCES INC.

THE LAST COUPLE OF decades has seen a rapid expansion in the application of random packings in distillation and absorption. At the same time, packing geometry has rapidly evolved from the simple shapes of the Raschig ring and Berl saddle to the multitude of sophisticated shapes now available. Today's packings have a more open structure and better aerodynamic contours than their predecessors and, therefore, give greater capacities and lower pressure drops.

The development of procedures for predicting packing performance has not kept up with the rate at which packing geometries have poured into the market. This has left the engineer with the dilemma of lots of packings from which to choose but few tools for evaluating their performance. The objective of our article is to narrow that gap. Specifically, we address packing capacity and present a new, generic procedure for predicting flood points and pressure drops of modern random packings.

H. Z. Kister is an engineering advisor leading the work on distillation and absorption at Brown & Root Braun, Alhambra, CA (818/300-4182; Fax: 818/300-3291). He is involved in the design, troubleshooting, revamping, control, and start-up of fractionation processes and equipment. Previously, he worked for ICI Australia and Fractionation Research, Inc. He received BS and MS degrees from the Univ. of New South Wales and is the author of the book "Distillation Operation" and a forthcoming book, "Distillation Design," as well as more than 30 technical articles.

D. R. Gill is a senior process engineer for Simulation Sciences Inc., Brea, CA (714/579-0412; Fax: 714/579-7468), where he provides technical support and training for simulation of refinery applications and processes. Prior to joining the firm, he was a process design engineer for C F Braun. A registered Professional Engineer, he holds a BS in chemical engineering and an MBA from California State Univ. at Long Beach.

Today's options

For several decades, the Sherwood–Leva–Eckert (SLE) correlation chart had been the standard of the industry for predicting flood points and pressure drops for random packing. The initial Sherwood version *(1)* contained only a flood curve. Leva *(2)* added to the chart a new family of curves for predicting pressure drops, while Eckert *(3,4)* made some further modifications. Perry's Handbook, 6th Ed. *(5)*, published in 1984, recommends one of Eckert's versions of the chart, Figure 1, as the sole correlation to use for flood and pressure-drop prediction for random packings.

The acceptance of the SLE chart has sharply declined during the past couple of decades. This prompted the appearance of a large number of alternative correlations. Most of these entirely abandoned the SLE chart, while others retained a few of the chart's features. Many attempted to substitute a more fundamental predictive model for the empiricism in the SLE chart.

Although many of these new correlations have shown promising results, none has gained industrywide acceptance for a number of reasons. Many are based on a limited body of data. Many only apply to a restricted range of packing geometries and have not been tested for other geometries. The limitations of these correlations often are unknown or, if known, seldom are reported. Many of the new models are still undergoing development.

Rather than developing yet another new correlation, we decided to take a fresh look at the prediction

31

method based on the SLE chart. We searched for the strengths of the SLE correlation that had made it the standard of the industry for so many decades and for its weaknesses that have recently caused it to fall out of grace. By evaluating the limitations of the SLE approach, we have been able to develop modifications that overcome its weaknesses.

Data bank

To evaluate and modify the SLE chart, a massive bank of flood, pressure-drop, and maximum-operational-capacity, MOC [defined per *(9)* as the maximum vapor rate that provides normal efficiency of a packing] data was assembled from the open literature.

Each set of raw pressure-drop data was available either as a tabulation or as a plot of pressure drop vs. vapor velocity at constant liquid rate or a constant reflux ratio. All tabulated data were converted into data plots. A vapor velocity corresponding to each discrete pressure drop on the SLE chart (0.1, 0.25, 0.5, 1.0, and 1.5 in. of water/ft of packing) was read off each pressure drop vs. velocity data plot. These data of vapor velocities at these discrete pressure drops were used in our work.

Uncertainties in flood-point definition (we counted 19 different definitions in the literature) and in interpreting pressure drops and maximum operational capacity were considered and discussed in detail elsewhere *(6)*. Not much could be done to alleviate these uncertainties because most data in the literature were unaccompanied by the relevant information such as the flood-point definition or whether a column was dry or wet packed. The only flood-point data screened out were those few data clearly related to a well-developed flood condition rather than incipient flooding. Pressure-drop data for columns 8 in. or less in diameter were also screened out because of the pronounced effect of column diameter on pressure drop for those smaller columns *(7,8)*.

In total, the data bank contained about 2,800 processed pressure-drop data points as well as about 200 flood and maximum-operational-capacity data points.

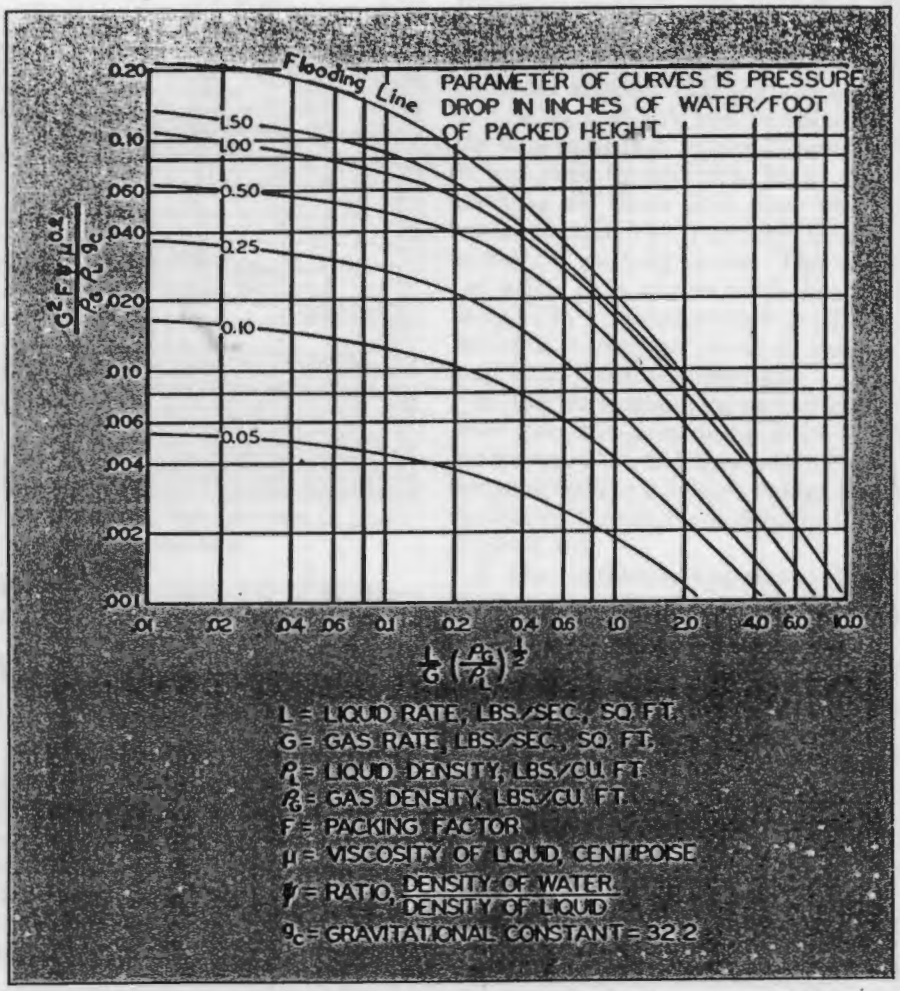

Figure 1. The version of the SLE correlation produced by Eckert and recommended in Perry's Handbook.

SLE data charts

Eckert *(4)* produced a later version of the SLE correlation chart than that given in Perry's Handbook and shown in Figure 1. The later version omitted the flood curve that appears in Figure 1 and also made some other minor adjustments. No reason was given for the omission of the flood curve; however, a possible explanation may become apparent from our evaluation. Strigle *(9)* changed the scales of Eckert's later version of the SLE correlation from log-log to semilog to make interpolation between adjacent pressure-drop curves easier. Strigle also updated packing factors based on Eckert's later version. Since there are only small differences between the two Eckert versions, we could have used either one but decided to go for the "best and latest" — *i.e.*, to use Strigle's semilog plot of Eckert's later version.

The abscissa of the correlation is known as the flow parameter:

$$X = \frac{L}{G}\left(\frac{\rho_G}{\rho_L}\right)^{0.5} \qquad (1)$$

The ordinate is the capacity parameter:

$$Y = C_s F_p^{0.5} \nu^{0.05} \qquad (2)$$

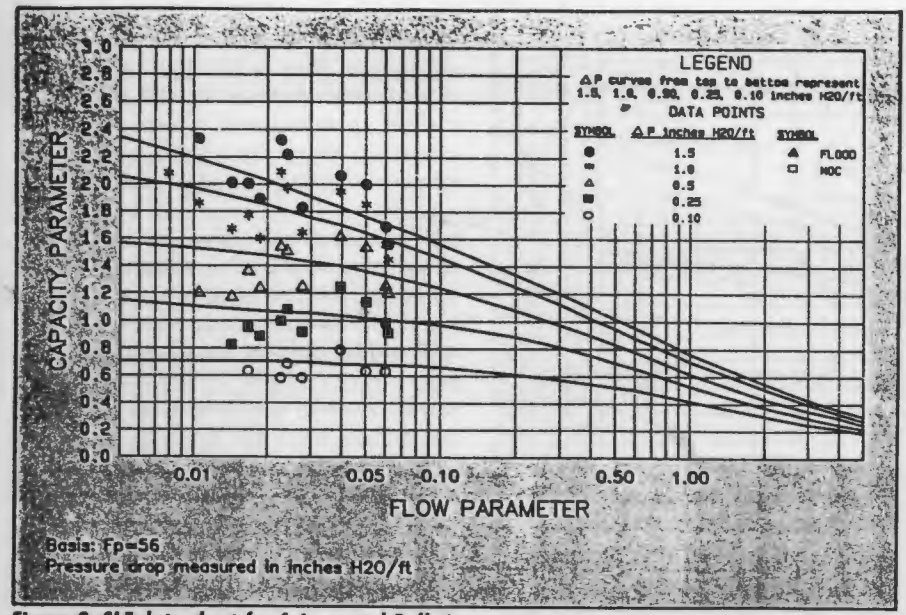

Figure 2. SLE data chart for 1-in. metal Pall rings, nonaqeuous systems, pressure drop only. Data from 9—20-in.-diameter test columns with packed heights of 4-10 ft.

where ν is the kinematic viscosity of the liquid and C_s is the superficial gas velocity corrected for vapor and liquid densities:

$$C_s = U_s\sqrt{\frac{\rho_G}{\rho_L - \rho_G}} \qquad (3)$$

F_p is the packing factor, which is an empirical value characteristic of the packing size and shape. Values of the packing factor are available in both the open and manufacturers' literature. To minimize inconsistencies among packing factors derived from different sources, we standardized on factors given in Strigle's recent book *(9)*. When the book did not provide a packing factor for a given packing, the manufacturer's literature was searched. Then, if the packing factor still could not be found, it was derived in a manner to give the best fit to available experimental data.

For each of the packings studied, the experimental pressure-drop, flood-point, and maximum-operational-capacity data were superimposed on the SLE correlation chart. We term the resulting charts, which contain both data and correlation curves, "SLE data charts." These charts allow a direct comparison of experimental data with correlation predictions. The entire set of charts is too extensive to fit in this article, but it will be included in a forthcoming book *(10)*. Figures 2–13 are typical, though.

Pressure-drop prediction: strengths and weaknesses

Comparing the experimental data with the predicted results clearly identified regions where the SLE correlation works well and regions where difficulties are encountered. The results of this analysis were then combined with experiences reported in the literature *(9,11,12)* to highlight the strengths and weaknesses of the SLE correlation:

1. Overall, the correlation fits the pressure-drop data well. Indeed, the agreement was excellent for 40% of the charts (*e.g.*, Figures 7 and 10), good for another 40% (*e.g.*, Figures 3–5, 8, 9, and 11), and reasonable for 15% more (*e.g.*, Figures 2 and 6). It was poor for only 5%. Many, including all those that gave poor matches, could be improved by altering the packing factors. This observation fully agrees with that of Strigle *(9)*, who showed that the SLE correlation gives an excellent statistical fit to pressure-drop data.

2. The correlation appears to give good pressure-drop predictions for most systems in the flow-parameter range of 0.05 to 0.3. Such values are typical of atmospheric distillation applications.

3. The correlation appears to give good pressure-drop predictions for the air/water system at atmospheric pressure throughout the entire flow-parameter range. Data for other aqueous systems also appear to agree well with correlation predictions, but there are insufficient data to draw a firm conclusion.

4. For nonaqueous systems, the correlation often tends to give optimistic pressure-drop predictions for flow parameters greater than 0.3, worsening as the flow parameter increases. This can be seen by compar-

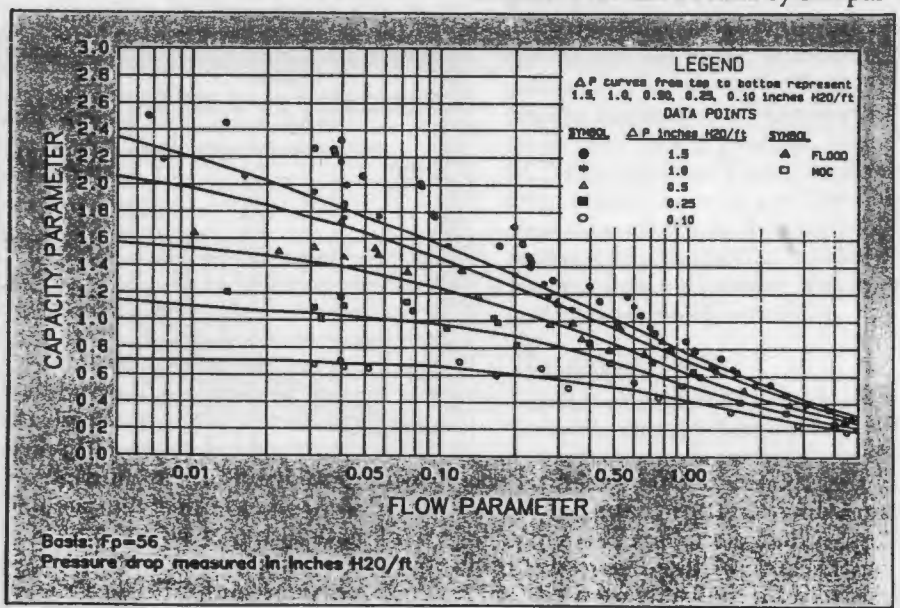

Figure 3. SLE data chart for 1-in. metal Pall rings, aqueous systems, pressure drop only. Data from 15—84-in.-diameter test columns with packed heights of 2—10 ft.

ing Figure 4 to Figure 5. Strigle *(9)* also observed these optimistic predictions. He attributed them to enhanced liquid frothiness at higher pressures. Because froth occupies more void space, pressure drop rises.

5. For nonaqueous systems, the SLE correlation tends to give optimistic predictions at flow parameters smaller than 0.03–0.05. This can best be seen by comparing Figures 2 and 3. In Figure 2, the data suggest that pressure drop is almost independent of the flow parameter and appears to be only a function of the capacity parameter.

Strigle *(9)* and Robbins *(12)* made similar observations. Robbins presents a thorough evaluation of pressure-drop prediction in this region, showing that at the low flow parameters, pressure drop is independent both of the flow parameter and of the liquid physical properties.

6. With some packings, the observed dependence of pressure drop on the flow parameter differs from that predicted by the SLE correlation, *e.g.*, Figure 9.

7. With some packings, the dependence of pressure drop on vapor velocity differs from that predicted by the correlation. See Figures 2 and 3.

8. With some packings, a rapid rise of pressure drop with vapor velocity occurs, but only at higher pressure drops and close to the flood point — *e.g.*, Figures 7–9 and 11. With large packings, this behavior appears to occur at relatively low pressure drops. We will discuss this tendency of large packings to flood at lower pressure drops later in this article.

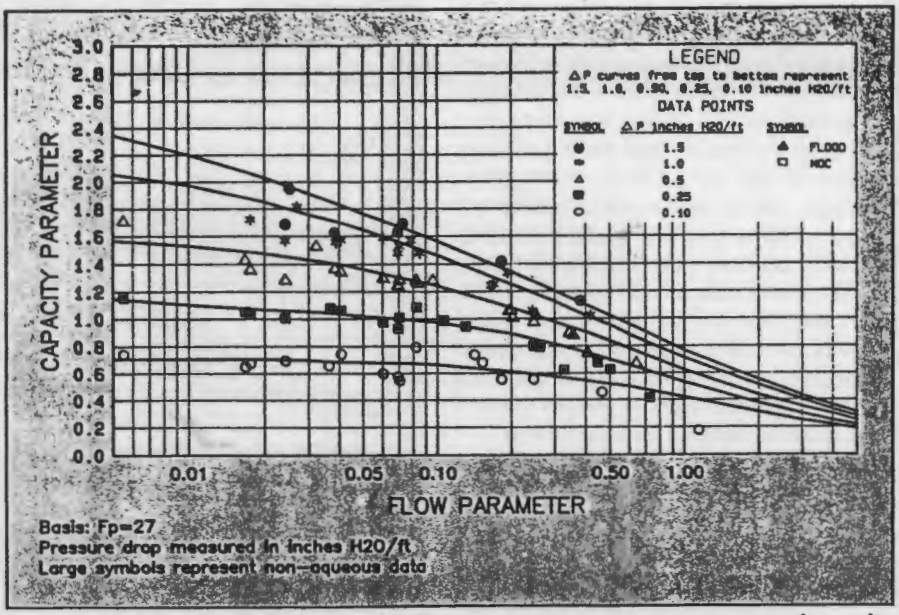

Figure 4. SLE data chart for 2-in. metal Pall rings, nonaqueous systems, pressure drop only. Data from 9–48-in. diameter test columns with packed heights of 40–20 ft.

9. The pressure-drop data fall consistently above or below the relevant curve for some packings, as seen in Figure 6. If this trend occurs throughout the diagram, it is indicative of a packing factor that is too high (data above the curves) or too low (data below the curves).

McNulty and Hsieh *(13)* discussed this limitation, pointing out the difficulties of setting packing factors due to their empirical nature. Strigle *(9)*, however, found that, for most packings, the packing factors appeared constant and neither too high nor too low. Strigle's finding is consistent with our observations.

10. Figure 3 shows a large scatter of pressure-drop data measured for a packing of a fixed shape (a Pall ring) and size (1 in.) using the same test system, air/water, at atmospheric pressure. This scatter reflects an inherent limitation of the pressure-drop data, not a problem with the SLE correlation. These data came from various sources and the scatter shows the effects of the origin of the packing, the method of packing the tower, column diameter, bed height, and experimental technique.

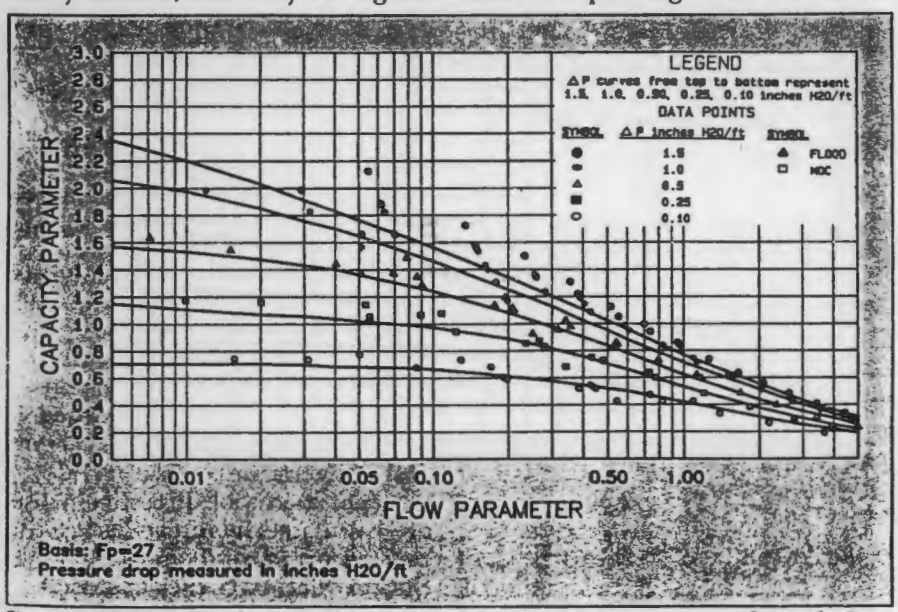

Figure 5. SLE data chart for 2-in. metal Pall rings, aqueous systems, pressure drop only. Data from 30—84-in.-diameter test columns with packed heights of 2—18 ft.

The implications

Both our current analysis and Strigle's clearly demonstrate that overall the SLE correlation gives good pressure-drop predictions. It is important to note the massive size of the data banks used both by ourselves and by Strigle.

Of great concern is that the limitations of the correlation tend to be systematic rather than random. Fur-

34

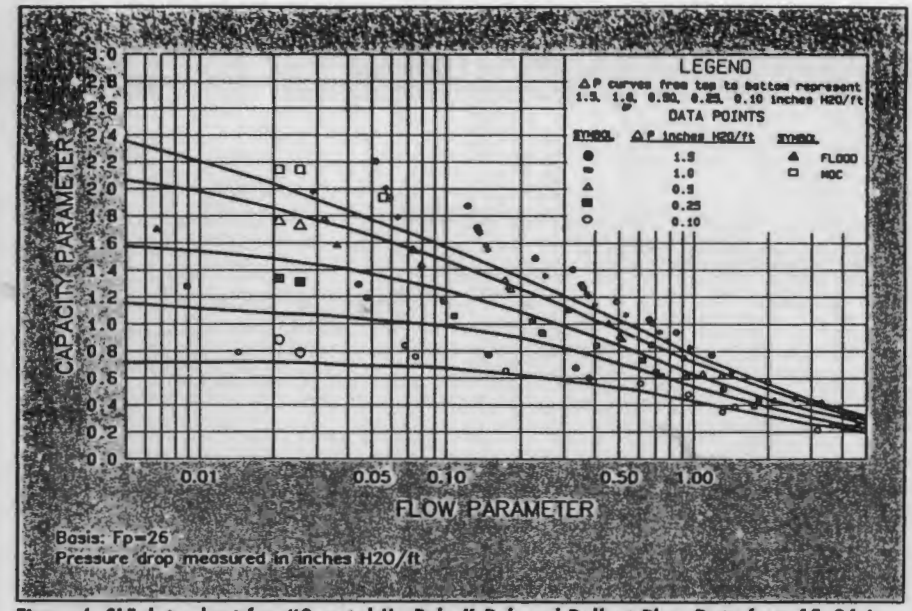

Figure 6. SLE data chart for #2 metal Hy-Pak, K-Pak and Ballast Plus. Data from 15–84-in.-diameter test columns with packed heights of 2–10 ft.

thermore, some of the regions where the correlation model tended to provide poor pressure-drop predictions are those of great commercial importance. The prime problem detected probably was the optimistic pressure-drop prediction for nonaqueous systems at high flow parameters. This region coincides with pressure-distillation and high-liquid-rate applications — a region in which random packings have made significant inroads in recent years. Another region of optimistic pressure-drop predictions is that of nonaqueous systems at low flow parameters. This coincides with vacuum-distillation and low-liquid-rate applications, which are again of great commercial significance. On the other hand, the correlation was found to work best for the air/water system, which is a system of little commercial interest.

Another concern is that, while the correlation works very well for some packings, it works poorly for others. The user has no way of readily telling (without comparing predictions to data) when the packing under consideration is one for which the correlation works poorly.

Finally, the effect of the inherent packing data limitations is of concern. Most data in the banks were obtained using small-scale equipment, with packing either wet packed or neatly dry packed. These conditions are conducive to low pressure drops *(6)*. In contrast, in commercial equipment the same packing is likely to produce a significantly higher pressure drop.

These concerns extend beyond an evaluation of the SLE correlation and are relevant to any packing pressure-drop correlation: A correlation is shown to give an excellent statistical fit to experimental data; yet, it gives unsatisfactory predictions for many situations commonly encountered in industrial practice. The conclusion is that even an excellent fit to experimental data is insufficient to render a packing pressure-drop correlation suitable for design. In addition to a good fit to the data, the correlation's limitations must be fully explored.

One additional implication of our evaluation of the SLE correlation is that it can serve as an invaluable analytical tool. Superimposing data on the curves of the correlation gives clear indication of where the correlation troublespots are and a good measure of their magnitude.

This analytical feature is a major advantage where correlation limitations are of prime importance. Utilizing this feature, we are able to improve the reliability of pressure-drop prediction.

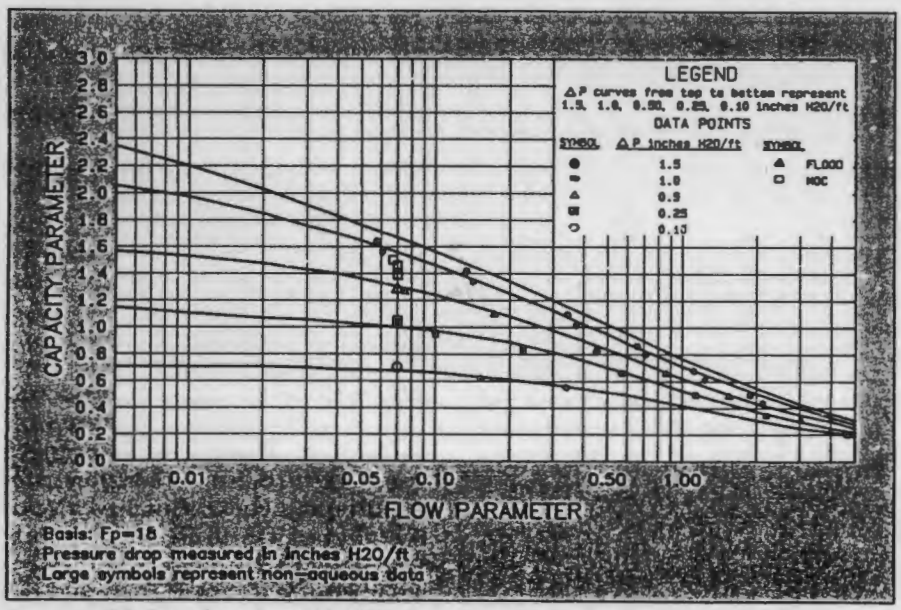

Figure 7. SLE data chart for #50 IMTP. Data from 15–30-in.-diameter test columns with packed heights of 10 ft.

An improved method

We do not propose any modifications to the contours or parameters of the SLE correlation. Instead, we recommend modifying the procedure of applying the correlation — to use the SLE data charts for predicting pressure drop. This essentially converts the correlation into an interpolation tool. Pressure drops are calculated by interpolating the plotted pressure-drop data, while the correlation curves are used to guide this interpolation. The mechanics are given in the sidebar.

35

How to Use the Procedure

Estimating flood and pressure drop using the SLE data charts essentially involves data interpolation and extrapolation within the framework of the Sherwood–Leva–Eckert correlation.

This technique should yield reliable predictions when appropriate data are available in the vicinity of the operating point. The reliability of the predictions diminishes in proportion to the extent that extrapolation is required. Whenever extensive extrapolation is necessary, the calculation should be abandoned because the predictions would be unreliable.

To use the method, follow the steps given here:

1. Select the appropriate SLE data chart for the packing being considered.

2. Using the operating or design conditions and the packing factor given on the chart, determine the operating point on the chart.

3. Check to see if the chart contains any data points in the vicinity of the operating point. If so, go to step 4. If not, look for the closest region that contains data. If this region is remote from the operating point, extrapolation is apt to be unreliable. Abandon the calculation and proceed to step 10. If the region is close, judiciously extrapolate the data near the operating point. Continue to steps 4 and 5, which give some guidelines. Bear in mind, though, that you are in an uncertain area and allow for this uncertainty.

4. Check to see if the data points in the vicinity of the operating point match the correlation. If so, obtain the pressure drop directly from the correlation curves and go to step 6. Otherwise, continue to step 5.

5. Draw a curve to fit the data points in the vicinity of the operating point. If the data points show a clear trend in this region, follow the data points. If no trend is apparent, draw the curve parallel to the correlation curve. Often, however, a compromise between the two is more appropriate. Some engineering judgment is needed here; a conservative estimate may be best.

6. Compare the nature of the operating system (aqueous or nonaqueous) to the nature of the data points used above. Keep in mind that aqueous data are derived almost entirely from the air/water system. If the operating system contains less than 50% water, it may behave much more like a nonaqueous system than an aqueous one. If the nature of the operating system is not the same as that for the plotted data points (or if using the extrapolation procedure in step 3), go to step 7. Otherwise, go to step 8.

7. Look for another SLE data chart that contains data for a system of the same nature as yours at the same operating point. Attempt to select a chart for a packing with as similar a packing factor and as similar a geometry to your choice as possible. Using the data from the second packing, obtain an estimate of the effect of the system's nature on pressure drop. If this effect is modest (say, less than 20%), correct the pressure-drop estimate for your packing. If the effect is 20% or more, the calculation is unreliable and should be abandoned; then go to step 10.

8. Check the range of column diameters and packing depths used to develop the data points in the chart and make a judicious estimate as to how well these data can be extended to your specific case. A more detailed description of the data sources and inherent uncertainties is available elsewhere *(6)*. Consider scaleup, packing technique, and other relevant factors. The scatter of the data around the curves in Figure 3 provides some sense of the magnitude of these factors. Adjust your estimate accordingly. Engineering judgment is needed here; a conservative estimate may be best.

9. Remember to review the comments in this article on the range of application of the SLE data charts. If any of the comments there apply to your case, be sure to allow for them. Then, your calculation is complete.

10. You have reached this step because you have had to abandon your calculation for the particular packing. So, request data on the packing in the vicinity of the operating point from its manufacturer, or consider an alternative packing for which there is more confidence in the performance prediction.

Keep in mind that, if you reached this step, you are in an uncertain region. The uncertainty is even greater if the system's nature has a considerable effect on packing pressure drop. Proceed only with extreme caution, recognizing that your calculation at best will be only an educated guess. It may pay to consider using the second packing instead because it offers more confidence in the reliability of the performance prediction.

The conversion of the SLE correlation into an interpolation chart overcomes all of the limitations outlined earlier. The data charts readily identify any regions where the data veer off the correlation curves, or where data are absent. When the data veer off the curves, pressure drop can be calculated by interpolation of the experimental data. Packing factors, often criticized for being inconsistent from one source to another, cease to be critical variables. Any inaccuracies in packing factors will be reflected as data deviations from the correlation curves and will be accommodated for by the interpolation procedure.

One can argue that the proposed procedure breaks down when data are absent. Even in such a case (and perhaps especially then), however, the user is better off than previously. The correlation curves are always there to fall back on for a prediction, but now the user clearly knows that there are no data for the region and, thus, that uncertainty is involved.

The SLE data charts permit comparative evaluation of different

packings based on actual experimental data at the desired operating point. The accuracy of a comparison is restricted only by the availability of experimental data and by the inherent data limitations. In the past, such a comparison involved either comparing packing factors, which is inaccurate, or a time-consuming analysis of experimental data.

Updating the SLE data charts is simple. All that needs to be done is to plot any new or additional data points on the charts. Likewise, it is easy to keep comparative records of previous design points.

The SLE data charts cannot overcome inherent data limitations. But even here the user is in a better position than before. Tabulations detailing data sources for each chart are available *(6)* and can be used to make an informed judgment about the uncertainty involved in extending the data to a specific application.

We searched for the strengths of the SLE correlation that had made it the standard of the industry for so many decades and for its weaknesses that have recently caused it to fall out of grace.

The only shortcoming of the procedure is that it replaces a single correlation chart with a multitude of diagrams. There are two problems here: First, the SLE charts consume more space in the design manual or on the computer and also require a greater updating effort. This, however, is a small price to pay for the added reliability and information. Second, only a selection of SLE data charts appear in this article. A much more comprehensive set of charts will appear in a forthcoming book *(10)*.

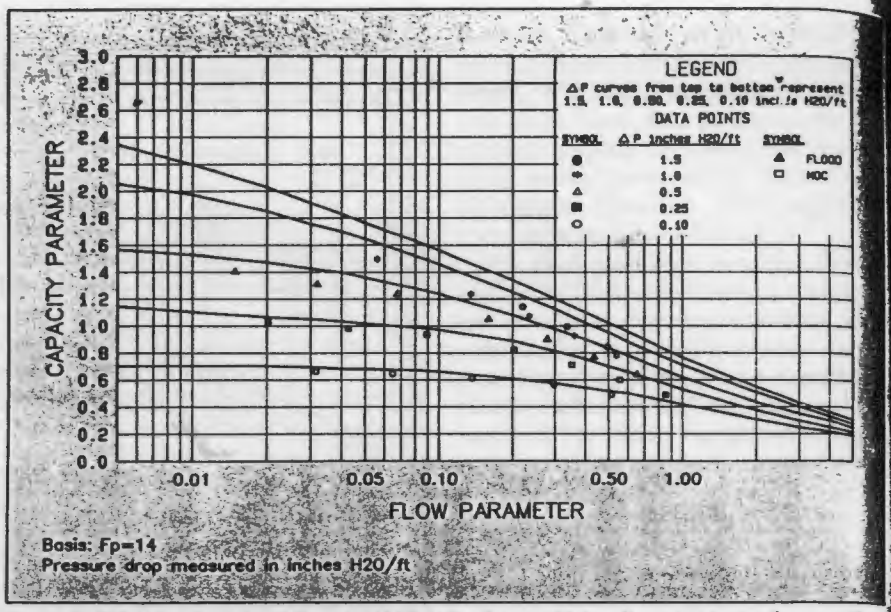

Figure 8. SLE data chart for #3 metal CMR. Data from a 36-in.-diameter test column with a packed height of 4 ft.

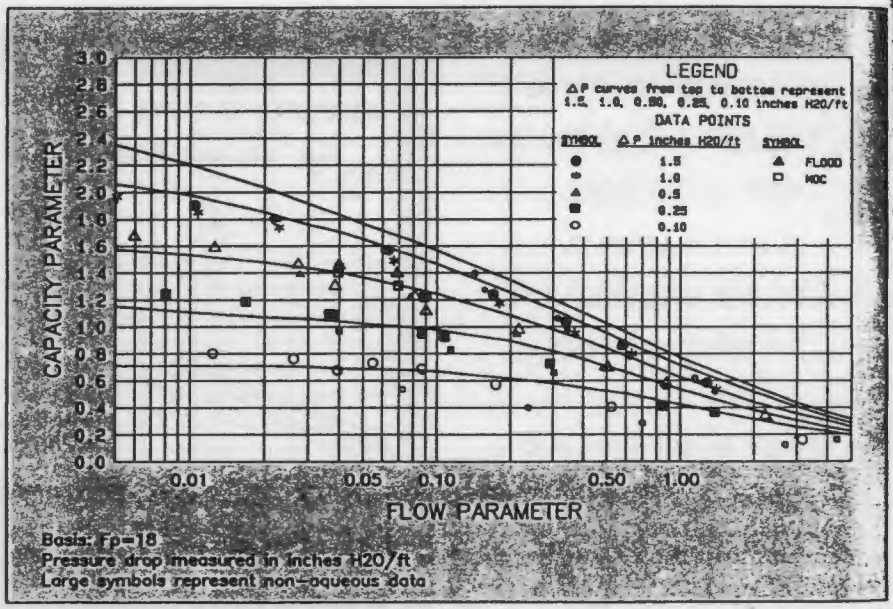

Figure 9. SLE data chart for #2 Nutter rings. Data from 20–48-in.-diameter test columns with packed heights of 4–14 ft.

Flooding prediction: strengths and weaknesses

The earlier Eckert version of the SLE correlation, Figure 1, included a flood curve located a short distance above the curve for a pressure drop of 1.5 in. of water/ft of packing. This implies that a column would flood when pressure drop reaches 2–4 in. of water/ft. This range has been confirmed for first-generation packings *(11,14)*. Figure 12 shows that, for smaller modern random packings, the flood point occurs at just below 2 in. of water/ft, *i.e.*, a slightly lower pressure drop than predicted in Figure 1. For larger modern packings, however, the flood point coincides with much lower pressure drop curves. This is best demonstrated by Figures 11 and 13. For such larger modern packings, the SLE correlation gives grossly optimistic flood-point predictions. These very optimistic pre-

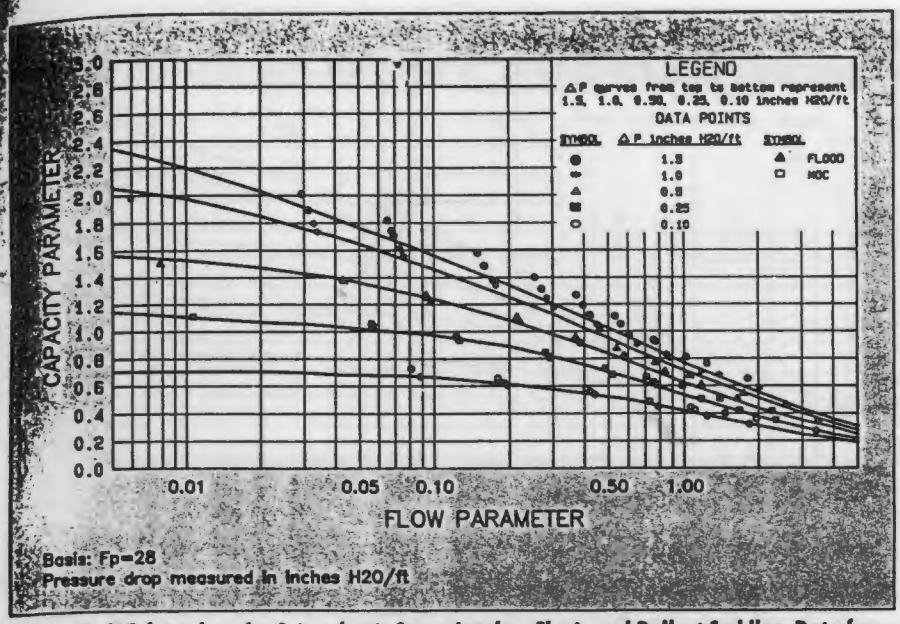

Figure 10. SLE data chart for 2-in. plastic Super Intalox, Flexi- and Ballast Saddles. Data from 30–84-in.-diameter test columns with packed heights of 2–10 ft.

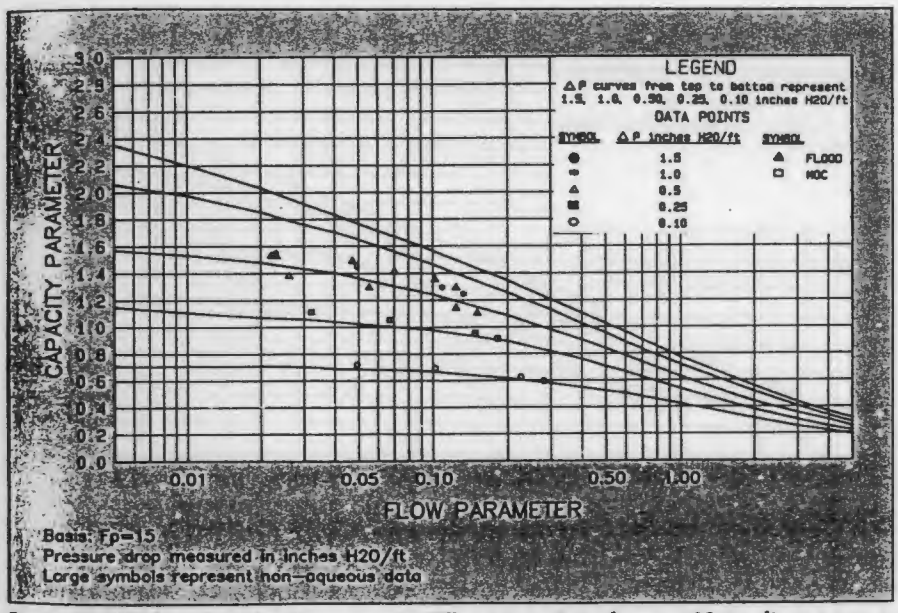

Figure 11. SLE data chart for 3-in. ceramic Hiflow rings. Data from an 18-in.-diameter test column with a packed height of 7 ft.

dictions were probably the reason why the flood curve was omitted from Eckert's later version of the SLE correlation.

Improving flood-point and MOC prediction

Figures 11–13 show that flood data correlate very well with the flow and capacity parameters. It therefore follows that these diagrams can be directly used as interpolation charts for accurate determination of flood point.

The same procedure also can be applied to MOC determination. We have noted that, for a given flow parameter, the MOCs typically are 5% lower, and seldom more than 10% lower, than the corresponding flood points. This can be seen in Figures 12 and 13. Therefore, assuming that the MOC occurs at a capacity factor that is 95% of the flood point is well within the accuracy of the prediction method. This will permit estimating MOCs from flood points and vice versa. It is worth emphasizing here that most flood data points in the literature appear to have been measured at incipient rather than fully developed flooding. This explains their proximities to MOCs.

For most packings, very few flood and MOC data have been reported. So, until more become available, it is practically impossible to use interpolation for predicting packing flood points and MOCs. Instead, a method for closely approximating packing flood points is needed and is derived below.

An excellent fit to experimental data is insufficient to render a packing pressure-drop correlation suitable for design. In addition, the correlation's limitations must be fully explored.

A close inspection of Figures 11–13 reveals that the pressure drop at the flood point is independent of the flow parameter, but varies both within a packing family and among packing types. This principle was discovered by Zenz *(14)* and, later, discussed by Strigle and Rukovena *(15)*. We now apply this principle to develop a new packing flood-point correlation.

Available flood pressure-drop data have been plotted against the relevant packing factors in Figure 14. The black squares are derived from our work; the stars show data from Zenz *(14)* and the circles indicate data from Strigle and Rukovena *(15)*. The relationship in Figure 14 can be expressed as:

$$\Delta P_{flood} = 0.115 F_p^{0.7} \qquad (4)$$

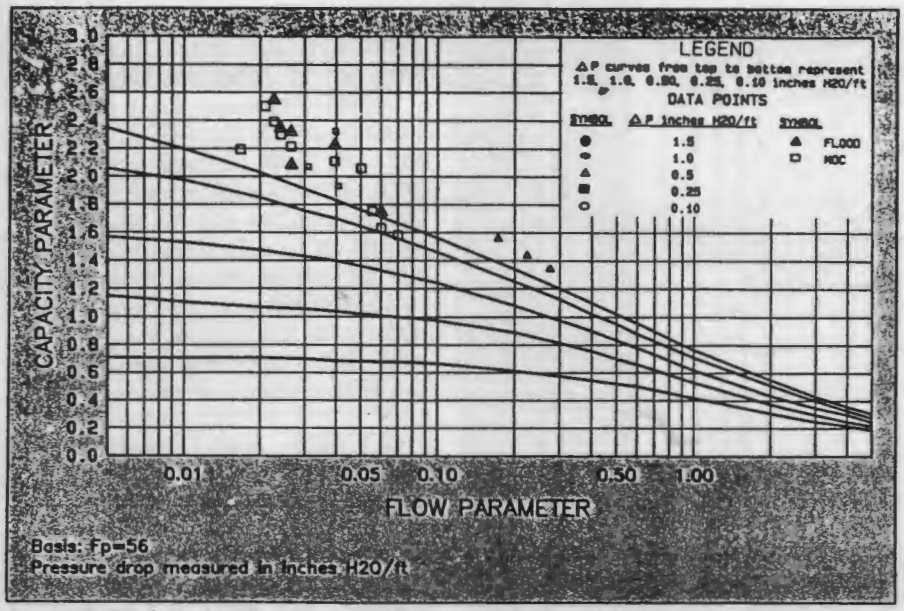

Figure 12. SLE data chart for 1-in. metal Pall rings, flood and MOC only. Data from 9–20-in.-diameter test columns with packed heights of 4–10 ft.

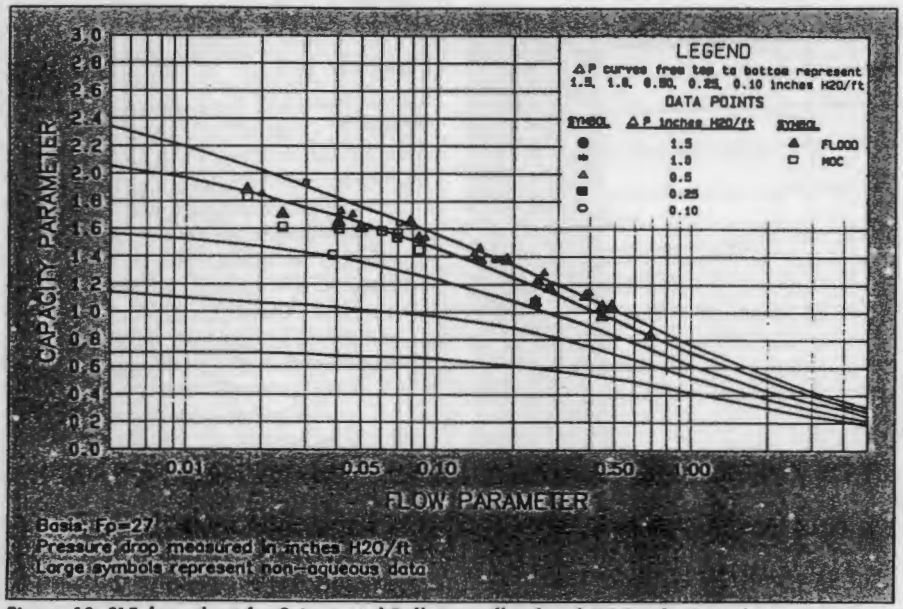

Figure 13. SLE data chart for 2-in. metal Pall rings, flood and MOC only. Data from 15–48-in.-diameter test columns with packed heights of 2–18 ft.

This equation permits estimation of the flood pressure drops for all random packings. Once this pressure drop is known, the flood velocity can be back-calculated using the SLE data charts.

Figure 14, which was used to develop Eq. 4, shows some scatter of data and, thus, has some inaccuracy. Inaccuracies in packing factors also will adversely affect the calculations. Both of these factors may lower the accuracy of the estimates for flood *pressure drop*. The flood-*velocity* calculation, however, is somewhat tolerant to inaccuracies in flood pressure drop. For instance, at a flood pressure drop of 1 in. of water/ft of packing, an error of 20% in the flood pressure drop calculated by Eq. 4 introduces an error of only about 4–8% in the flood-velocity calculation. Furthermore, the effect of packing factor on the flood pressure drop acts in an opposite direction to the effect of packing factor on the flood velocity. So, the impact of packing factor on flood velocity will be minimized. It therefore appears that the flood velocity calculated using Eq. 4, and the procedure proposed here, will be reasonably insensitive to inaccuracies in the equation or in the packing factors.

On the other hand, it is important to note that, except for one point in Figure 14, the lowest packing factor used to derive Eq. 4 is 14. We therefore do not recommend extrapolation of the equation to values lower than 14.

Figure 14 shows that when the packing factor exceeds 60, the flood pressure drop exceeds 2 in. of water/ft of packing, coinciding with the flood curve on Eckert's correlation, Figure 1. This explains why Eckert's correlation works well for low-capacity packings (*e.g.*, first-generation ones and smaller modern packings). Larger modern random packings typically have packing factors of between 15 and 30, and, so, their flood pressure drops are much lower, 0.7–1.3 in. of water/ft of packing. Therefore, Figure 1 provides optimistic predictions.

Figure 15 compares flood points calculated using the procedure based on Eq. 4 with experimental data for various packings. Almost all

NOMENCLATURE

C_s	=	superficial gas velocity, see Eq. 3, (ft/s);
F_p	=	packing factor, an empirical value depending on packing shape and size, ft^{-1};
G	=	gas mass flow rate, (lb/s · ft^2);
L	=	liquid mass flow rate, (lb/s · ft^2);
MOC	=	maximum operational capacity; per *(9)*: the maximum vapor rate that provides normal efficiency of a packing;
U_s	=	gas superficial velocity, (ft/s);
ΔP	=	pressure drop, in. of water/ft of packing;
X	=	flow parameter defined by Eq. 1;
Y	=	capacity parameter defined by Eq. 1;
ρ_G	=	gas density, (lb/ft^3);
ρ_L	=	liquid density, (lb/ft^3);
ν	=	liquid kinematic viscosity, (centistokes);
flood (subscript)	=	at the flood point.

the data are predicted to within 15%, most to within 10%. This demonstrates the suitability of the procedure for flood-point estimates.

Figure 16 extends the analysis to MOCs. Experimental MOC data are plotted against values calculated by applying Eq. 4 (for estimating the flood-point velocity) and assuming that the MOC occurs at 95% of the flood-point velocity. Almost all of the data are predicted to within 20%, and most are within 15%. This somewhat lower accuracy is to be ex-

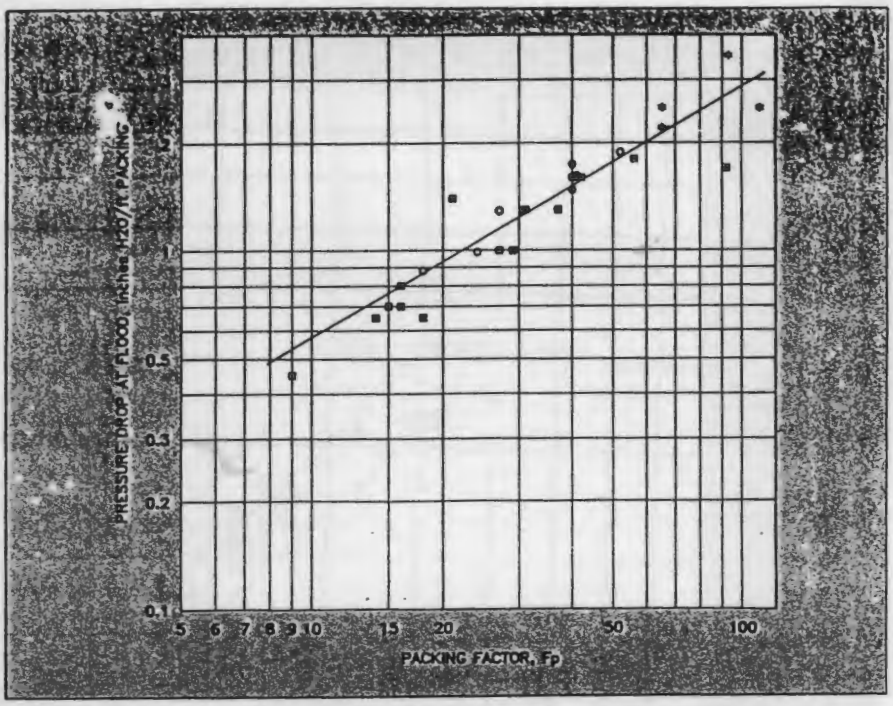

Figure 14. Flood pressure drop vs. packing factor for random packings.

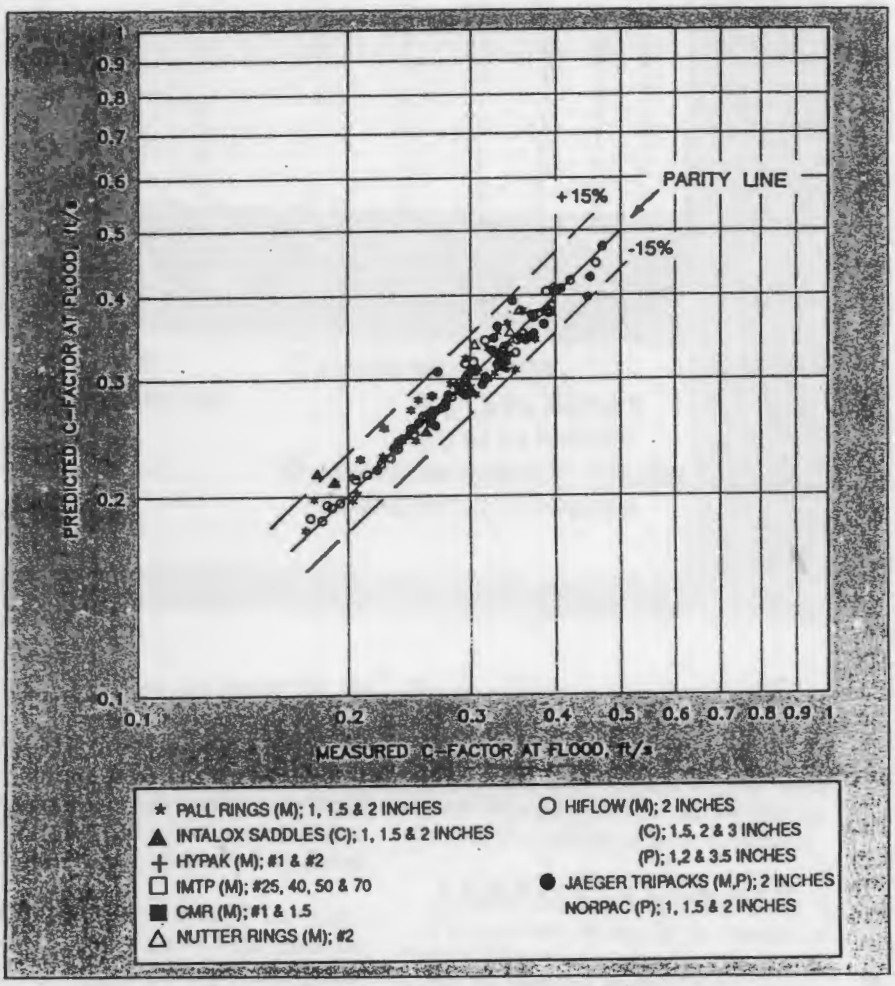

Figure 15. Predictions for flood based on Eq. 4 vs. experimental data.

LITERATURE CITED

1. **Sherwood, T. K., G. H. Shipley, and F. A. L. Holloway,** *Ind. Eng. Chem.*, **30** (7), p. 765 (1938).
2. **Leva, M.,** *Chem. Eng. Progress Symposium Series*, **50** (10), p. 51 (1954).
3. **Eckert, J. S.,** *Chem. Eng. Progress*, **66**, p. 39 (March 1970).
4. **Eckert, J. S.,** *Chem. Eng.*, April 14, 1975, p. 70.
5. "Chemical Engineer's Handbook," 6th Ed., McGraw-Hill, New York (1984).
6. **Kister, H. Z., and D. R. Gill,** "Flooding and Pressure Drop Prediction for Modern Random Packings," presented at the AIChE Spring National Meeting, Orlando, FL (March 1990).
7. **Billet, R., and J. Mackowiak,** *Verfahrenstechnik*, **16**, p. 67 (1982).
8. **Billet, R.,** "Packed Tower Analysis and Design," Ruhr University, Bochum, Germany (1989).
9. **Strigle, R. F.,** "Random Packings and Packed Towers," Gulf Publishing, Houston (1987).
10. **Kister, H. Z.,** "Distillation Design," in press, McGraw-Hill, New York (expected to be published in 1992).
11. **Bolles, W. L., and J. R. Fair,** *I. Chem. E. Symposium Series*, **56**, p. 3.3/35 (1979).
12. **Robbins, L. A.,** "A New Generalized Pressure Drop Correlation for Packed Towers," presented at the AIChE Spring National Meeting, Orlando, FL (March 1990).
13. **McNulty, K. J., and C. L. Hsieh,** "Hydraulic Performance and Efficiency of Koch Flexipac Structured Packings," presented at the AIChE Annual Meeting, Los Angeles, CA (November 1982).
14. **Zenz, F. A.,** *Chem. Eng.*, August 1953, p. 176.
15. **Strigle, R. F., and F. Rukovena,** *Chem. Eng. Progress*, **75**, p. 86 (March 1979).

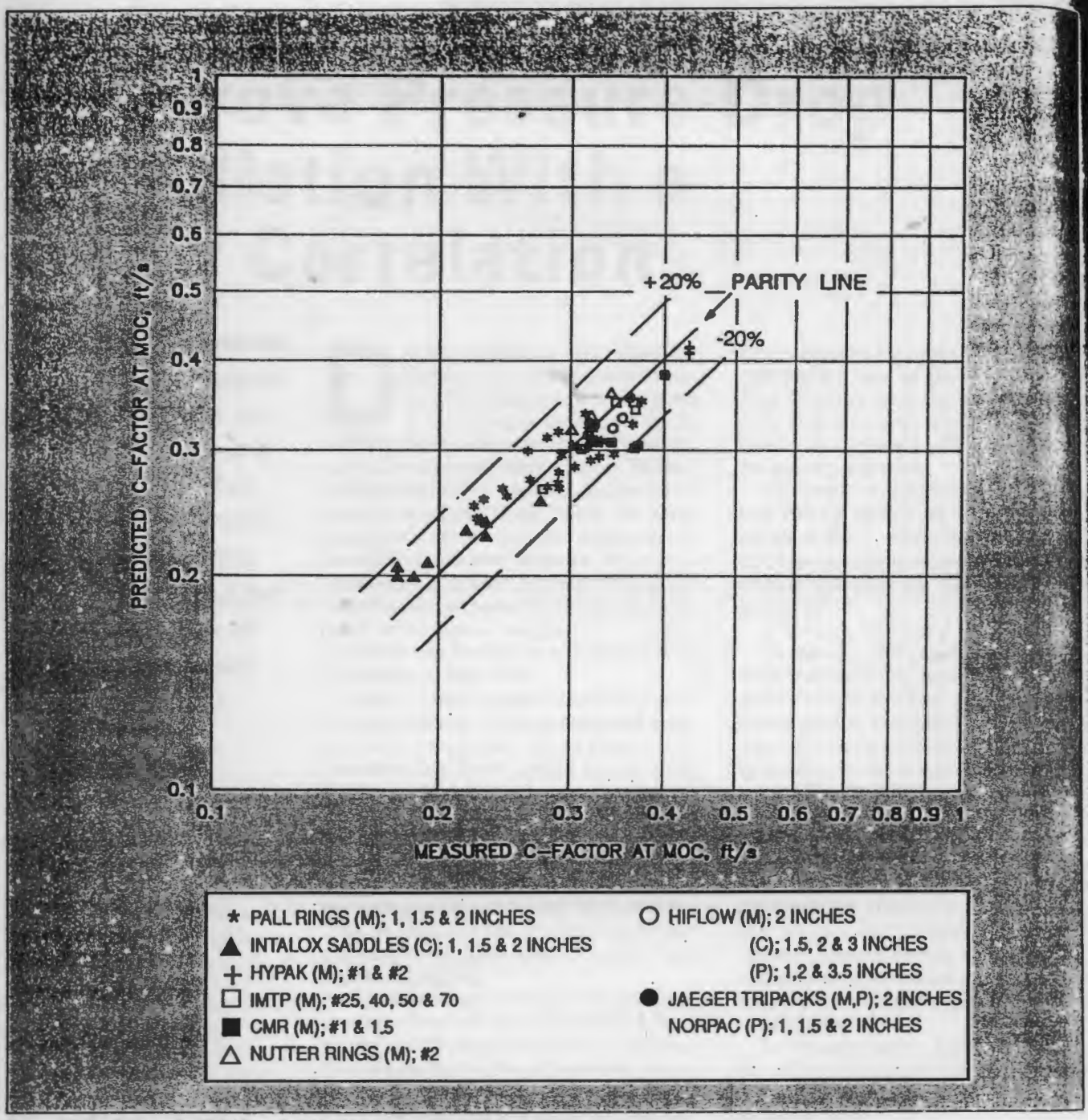

Figure 16. Predictions for MOC based on Eq. 4 vs. experimental data.

pected given the additional approximation used.

Limitations

While the procedure we have introduced overcomes the limitations of the SLE *correlation*, it does not surmount the limitations inherent in the flood and pressure-drop *data*. Predictions based on SLE data charts will only be as good as the data on which they are based. So, we strongly recommend that the SLE data charts only be used once the user is familiar with the data limitations and can reasonably evaluate their impact on chart prediction. These points are discussed in detail elsewhere *(6)*.

All data were derived for nonfoaming systems and in the absence of corrosion, breakage, compression, and chipping of packings. Pressure drop is considerably higher in a foaming system and when packings have been deformed or damaged, and, therefore, the SLE data charts would provide optimistic estimates if applied to such systems.■

ACKNOWLEDGMENT

The authors thank D. E. Nutter of Nutter Engineering for his kind assistance in making unpublished, large-scale simulator data available.

41

Improve Pressure-Drop Prediction With a New Correlation

This generalized correlation for packed towers uses dry-bed packing factors. Such factors are provided for more than 90 commercial packings.

Lanny A. Robbins
The Dow Chemical Co.

Design criteria for calculating the diameter of a packed tower for absorption, stripping, rectification or fractionation depend primarily on the hydraulic characteristics of pressure drop, flooding and entrainment. The existing correlations used for design, however, have serious flaws. Here, we introduce a new correlation that avoids them. In addition, this new pressure-drop correlation enhances our understanding about where a packed tower is operating in regards to the liquid- and gas-flow regimes, and about the sensitivity of pressure drop to changes in flow rates.

Eckert *(1)* and Strigle *(2)* have reviewed the development of the generalized pressure-drop correlation, which started with flooding data from packed towers with countercurrent flow of vapor and liquid. By experience, the packing was observed to flood when the pressure drop was in the range of 2 in. H_2O/ft. Consequently, towers have been designed to operate at some percentage of flooding, say 50% to 80%. This, in turn, has led to operation in the pressure drop range from 0.2 to 0.7 in. H_2O/ft of packing.

A natural improvement for correlating pressure-drop data was to generate a family of curves beneath the flooding correlation at constant values of pressure drop, *e.g.*, 1.5, 1.0, 0.5, 0.1, and 0.05 in. H_2O/ft. This, however, led to a problem that has needed to be resolved — and is by the new correlation.

Dry-bed pressure drop

For a tower to flood, two phases must be present (a vapor and a liquid in this case), and the heavy phase (liquid) should pass down the packing countercurrent to the upflow of the light phase (gas). Flooding depends on the flow rates, the properties of the liquid and gas, and the geometry of the packing. But at low liquid loadings — and especially when the bed is dry — pressure drop may occur simply because of the flow of gas through the bed. This pressure drop depends on the gas flow rate, the gas properties, and the geometry of the tower packing, but not on the liquid properties.

The pressure drop across a dry, packed bed can be correlated with the orifice equation, Eq. 1, where the pressure drop, ΔP, is proportional to the gas density, ρ_g, and the square of the superficial gas velocity, V_s^2:

$$\Delta P = C_o \rho_g V_s^2 = C_o F_s^2 = C_o G^2/\rho_g \quad (1)$$

In contrast, the generalized pressure-drop correlation presented by Eckert *(1)* and by Strigle and Norton Co. *(2,3)* uses liquid density and liquid viscosity even where the liquid properties have practically no effect on the pressure drop. It correlates ΔP with the flooding parameter, $F_p[G^2/\rho_g][\mu^{0.1}/(\rho_L - \rho_g)]$, even when the packing is essentially dry, *i.e.*, at low values of L/G. Similarly, the pressure-drop curves presented by Glitsch *(4)* correlate ΔP with $[G^2/\rho_g]\,[1/(\rho_L - \rho_g)]$ even for a dry bed. The dry-bed pressure drop would be expected to correlate with G^2/ρ_g, but clearly should not be expected to correlate with the properties of some liquid that is not actually present.

In one correlation, Leva *(5)* modified the orifice equation by adding the effect of the superficial liquid velocity, V_L, in an exponential term:

$$\Delta P = C_o \rho_g V_s^2 10^{C1 V_L} \quad (2)$$

This is satisfactory because there is no effect from liquid properties when the liquid flow rate is zero, but the correlation is limited to low values of ΔP and V_L where the log-log correlation gives straight lines. Leva *(5)* correlated specific values of C_o and C_1 for each packing. Since that time, however, many new packings have been developed. Eckert *(1)* updated the list of packing factors from air/water pressure-drop data and the generalized pressure-drop correlation.

42

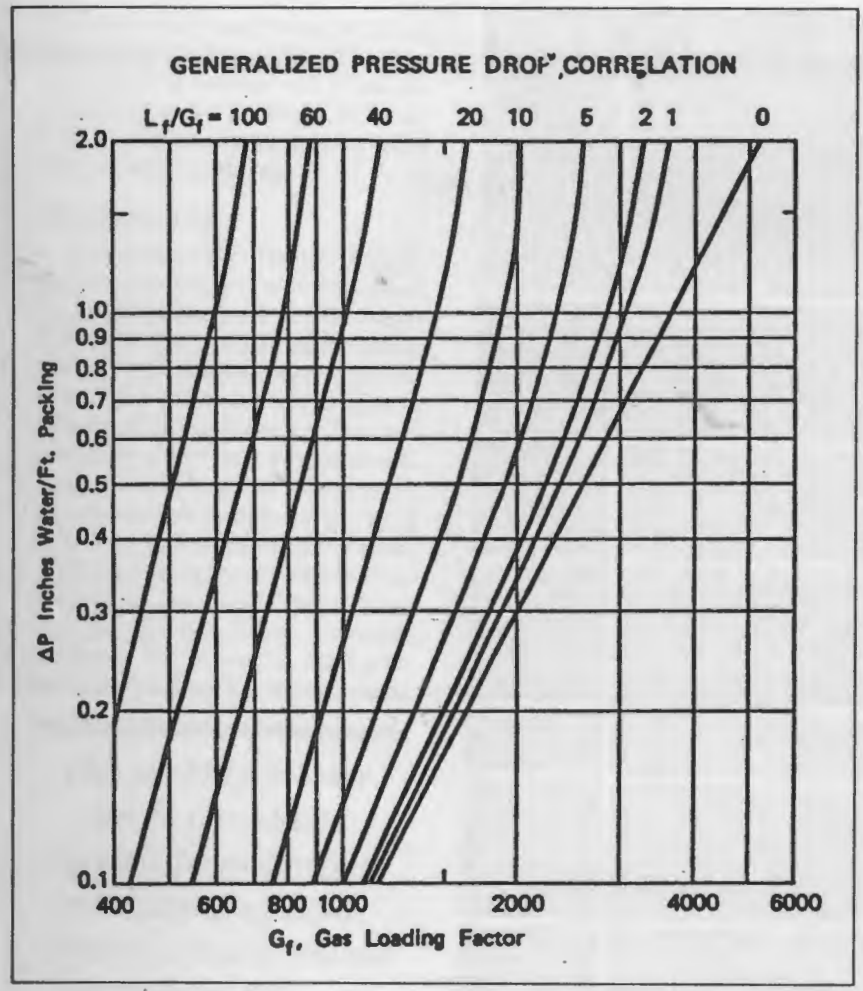

■ *Figure 1. Pressure drop response to liquid and gas loadings.*

The solution

To avoid the problem, we introduce an improved, generalized pressure-drop correlation that starts with the dry-bed pressure drop, which depends on the gas properties alone. Then, the influence of the liquid flow rate and liquid properties are added.

The lists of C_o and C_1 in Eq. 2 provided by Leva *(5)* were extended to include the modern packings. Upon analysis, the values of C_o were found to correlate directly with values of the packing factor, F_p. The beauty of this observation is that the packing factors can be correlated directly from dry-bed pressure-drop data, which normally fall on a straight-line plot of log ΔP vs. log G with a slope of 2.0. On further investigation, the values of C_1 in Eq. 2 were found to correlate reasonably well with the square root of the packing factor and the liquid viscosity to the 0.1 power.

At low liquid loadings, pressure drop may occur simply because of the flow of gas through the bed.

This leads to the formulation of a new generalized pressure-drop correlation, Eq. 3:

$$\Delta P = C_3 G_f^2\, 10^{C_4 L_f} + 0.4[L_f/20{,}000]^{0.1}[C_3 G_f^2 10^{C_4 L_f}]^4 \quad (3)$$

where

$$G_f = G[0.075/\rho_g]^{0.5}[F_{pd}/20]^{0.5} = 986 F_s[F_{pd}/20]^{0.5} \quad (4)$$

and

$$L_f = L[62.4/\rho_L][F_{pd}/20]^{0.5}\mu^{0.1} \quad (5)$$

The first part of the correlation covers the straight-line correlation of log ΔP vs. log G with a slope of 2.0 when ΔP is below 0.5 and L_f is below 20,000. The second part describes the increase in slope of ΔP vs. G_f up to the flood point when liquid is flowing down the tower and the ΔP is above 0.5 in. H_2O/ft.

Use the following approximations, as required:

- For operating pressures above 1 atm, multiply the values of G_f in Eq. 4 by $10^{0.3}\rho^g$, or a similar factor, to predict higher pressure drop as the critical pressure is approached.
- For small packings where F_{pd} is 200 or more, L_f depends more heavily on liquid viscosity because of liquid bridging the small void spaces; so, substitute $\mu^{0.2}$ in Eq. 5.
- For large packings where F_{pd} is below 15, L_f appears to depend on the inverse of the packing factor; use $(20/F_{pd})^{0.5}$ in Eq. 5.

The pressure-drop data for curve fitting Eq. 3 were taken from the air/water pressure-drop curves from vendor data sheets. The new correlation now provides a uniform basis for comparing all packings. By definition, the dry-bed pressure drop can be described mathematically via Eq. 6.:

$$F_{pd} = 2.7 \times 10^8[\rho_g/0.075][\Delta P_{db}/G^2] = 278\Delta P_{db}/F_s^2 \quad (6)$$

Dry-bed pressure-drop data for more than 90 different packings were correlated with gas rates using Eq. 6

L. A. ROBBINS is a senior research scientist for The Dow Chemical Co., U.S.A., Midland, MI 48667 (517/636-1939, Fax: 517/636-4616). He has worked in pilot-plant research since receiving his Ph.D. in chemical engineering from Iowa State Univ. He is the author of the liquid-liquid extraction chapters in Perry's Chemical Engineers' Handbook, 6th Ed., and the Handbook of Separation Techniques for Chemical Engineers, 2nd Ed.

over a pressure drop range of 0.1 to 0.5 in. H_2O/ft of packing. The dry-bed packing factors are listed in Table 1 for metal packings, in Table 2 for plastic packings, and in Table 3 for ceramic packings.

Observations

One interesting point to note is that the dry-bed pressure-drop lines for similar packings, *e.g.*, 2-in. metal Pall rings, 2-in. metal Ballast rings, and 2-in. metal Flexirings, differed. Part of this might have been due to differences in the diameter of the test towers, and part may be due to differing bed heights used. Another interesting point is that the packing factors or packing densities of some of the short height-equivalent-to-a-theoretical-plate (HETP) packings changed as the tower diameter changed. For example, the 1/4-in. Protruded packing exhibited a packing factor of 1,390 in a 2-in. tower, vs. about 1,010 in 4-in. and 6-in. towers, and about 700 in a 12-in.-diameter one. The Goodloe knitted-wire-mesh packing exhibited a packing factor of about 240 in a 1-in. tower, compared to about 140 in a 3-in. one, and about 50 in a 12-in. tower. Presumably, the packing was squeezed to higher densities in the smaller-diameter towers. For large-diameter towers, the Goodloe packing density is controlled at 26.8 lb/ft^3 to maintain consistent quality, which likely maintains the pressure-drop packing factor close to 50.

The packing factors can be correlated directly from dry-bed pressure-drop data, which normally fall on a straight-line...

As all of the data are evaluated further and the dependence on liquid loading is carefully scrutinized, subtle adjustments may be recommended in the constant, C_4, used with L_f in Eq. 3 for some packings. The constant, C_3, used with G_f should, how-

Table 1. Dry-Bed Packing Factors For Metal Packings.

Size	Packing	Tower Dia., In.	Fpd	Reference
1/4 in.	Raschig Rings 1/32 in.	—	700*	1
1/2 in.	Raschig Rings 1/32 in.	—	300*	1
1 in.	Raschig Rings 1/16 in.	30	150	3
1-1/2 in.	Raschig Rings 1/16 in.	30	84	3
2 in.	Raschig Rings 1/16 in.	30	68	3
5/8 in.	Pall Rings	15	80	3
1 in.	Pall Rings	30	53	3
1 in.	Ballast Rings	84	37	4
1-1/2 in.	Pall Rings	30	28	3
1-1/2 in.	Ballast Rings	84	30	4
2 in.	Pall Rings	30	24	3,11
2 in.	Flexirings	36	25	13
2 in.	Ballast Rings	84	19	4
3-1/2 in.	Ballast Rings	84	14	4
No. 1	Hy-Pak	30	40	9
No. 1-1/2	Hy-Pak	30	26	9
No. 2	Hy-Pak	30	17	9
60 mm	Ballast Plus Rings	84	14	4
No. 3	Hy-Pak	30	13	9
No. 1	Chempak	14	29	19
No. 2	Chempak	14	17	9
No. 0	Cascade MiniRing	—	55*	24
No. 1	Cascade MiniRing	—	31	24
No. 2	Cascade MiniRing	—	24	24
No. 3	Cascade MiniRing	—	13	24
No. 4	Cascade MiniRing	—	9.8	24
15 mm.	Intalox	—	51	8
25 mm.	Intalox	15	43	8
40 mm.	Intalox	15	26	8
50 mm.	Intalox	15	17	8
No. 0.7	Nutter Ring	30	39	10
No. 1.0	Nutter Ring	30	27	10
No. 1.5	Nutter Ring	30	20	10
No. 2.0	Nutter Ring	30	17	10
No. 2.5	Nutter Ring	30	15	10
No. 3.0	Nutter Ring	30	11	10
Type 1	Flexipac	36	32	13
Type 2	Flexipac	36	11	13
Type 3	Flexipac	36	4.5	13
Type 4	Flexipac	36	3.2	13
1/4 in.	Protruded	2	1,390	22
1/4 in.	Protruded	4 & 6	1010	22
1/4 in.	Protruded	12	700	22
	Typerfil	6	140	20
	Goodloe	1	240	17
	Goodloe	3	140	17
26.8 lb/ft^3	Goodloe	12	50	18
	Montz A-2	20	23	19
	Koch-Sulzer (BX)	20	16	16
	Neo-Kloss	8	6	21
	Glitsch Grid	84	5	4

* Published F_p, no DP data available.

Table 2. Dry-Bed Packing Factors For Plastic Packings.

Size	Packing	Tower Dia., In.	Fpd	Reference
5/8 in.	Pall Rings	15	106	3
1 in.	Pall Rings	30	55	3
1 in.	Ballast Rings	84	42	4
1-1/2 in.	Pall Rings	30	40	3
1-1/2 in.	Ballast Rings	84	34	4
2 in.	Pall Rings	30	25	3
2 in.	Ballast Rings	84	20	4
3-1/2 in.	Pall Rings	30	12	3
3-1/2 in.	Ballast Rings	84	13	4
1A	Cascade MiniRing	—	28	24
2A	Cascade MiniRing	—	28	24
3A	Cascade MiniRing	—	10	24
No. 1	Super Intalox Saddles	15	40	3
No. 1	Ballast Saddles	84	49	4
No. 2	Super Intalox Saddles	30	26	3
No. 2	Ballast Saddles	84	23	4
No. 3	Super Intalox Saddles	30	14	3
No. 3	Ballast Saddles	84	14	3
No. 2	Levapacking	14	16	25
2 in.	Tri-Packs	24	13	23
No. 1	Tellerettes	—	40	26

Table 3. Dry-Bed Packing Factors For Ceramic Packings.

Size	Packing	Tower Dia., In.	Fpd	Reference
1/4 in.	Raschig Rings	—	1,600*	1
3/8 in.	Raschig Rings	—	1,000*	1
1/2 in.	Raschig Rings	—	520	15
1 in.	Raschig Rings 1/8 in.	30	150	3
1-1/2 in.	Raschig Rings 3/16 in.	30	80	3
2 in.	Raschig Rings 1/4 in.	30	70	3
No. 2	Cascade MiniRing	—	38*	24
No. 3	Cascade MiniRing	—	24*	24
No. 5	Cascade MiniRing	—	18*	24
1/4 in.	Berl Saddles	—	900*	1
1/2 in.	Berl Saddles	—	274	14
3/4 in.	Berl Saddles	—	142	14
1 in.	Berl Saddles	—	94	14
1-1/2 in.	Berl Saddles	—	47	14
2 in.	Berl Saddles	36	31	14
1/4 in.	Intalox Saddles	8	830	12
1/2 in.	Intalox Saddles	15	187	3
3/4 in.	Intalox Saddles	15	132	3
1 in.	Intalox Saddles	30	94	3
1-1/2 in.	Intalox Saddles	30	50	3
2 in.	Intalox Saddles	30	37	3
3 in.	Intalox Saddles	30	20	3
No. 1	Super Intalox Saddle	30	62	3
No. 2	Super Intalox Saddles	30	31	3

*Published F_p, no DP data available.

ever, remain fixed by definition, and then the value of the dry-bed packing factor can be determined by correlation with dry-bed pressure-drop data in the range from 0.1 to 0.5 in. H_2O/ft.

For the design of packed towers, Eq. 3 can be used when L_f is below 20,000, but requires a trial-and-error solution. Therefore, Figure 1 was developed as a graph of the new generalized pressure-drop correlation including liquid loading factors above 20,000. Figure 1 and Eq. 3 can be used for all packings. If there is a concern about the effect of liquid loading on one specific packing, however, one can use the air/water pressure-drop curves for that specific packing, and redefine the water loading as being equal to $L(62.4/\rho_L)\mu^{0.1}$ and the air loading as being equal to $G(0.075/\rho_g)^{0.5}$.

Table 4. Packed Tower Pressure Drop Increase Due To Liquid Loading.

Lf	10 (2.7 x 10-5)Lf
500	1.03
1,000	1.06
1,500	1.10
3,000	1.21
5,000	1.36
10,000	1.86
20,000	3.47

Table 4 shows that tower packings essentially operate at the dry-bed pressure drop when the liquid loading factor is below 1,500 (equivalent to 3 gal/min/ft² at $F_p = 20$). The pressure drop is within 10% of the dry-bed pressure drop. This condition exists in the rectification section of many towers, especially in vacuum rectification at low pressure drop.

The pressure drop at flooding can be predicted with the relationship shown by Kister and Gill *(6)* in Eq. 7:

$$\Delta P_{flood} = 0.115\ F_p^{0.7} \qquad (7)$$

They reported that the maximum operational capacity, MOC—defined by Strigle (2,7) as the maximum vapor rate that provides normal efficiency of a packing—occurs at about 95% of the flood point velocity that gives the ΔP_{flood} in Eq. 7. CEP

45

How to Determine the Diameter of a Packed Column

The following procedure is now recommended for properly sizing the diameter of a packed tower.

1. First, specify the liquid and vapor flow rates to be used based on the stripping factor, absorption factor, or reflux ratio desired.
2. Determine the liquid density, the vapor density, and the liquid viscosity.
3. Select the pressure drop to be designed into the tower operation. Most packed towers operate below 1.0 in. of water pressure drop per foot of packing. Atmospheric and pressure distillations are usually designed for 0.5 to 0.7 in. H_2O/ft. Absorbers and strippers (regenerators) are often designed for 0.2–0.6 in. H_2O/ft. The lower ΔP is used for design if foaming occurs or if fan horsepower needs to be minimized. Vacuum distillations are frequently designed to operate in the range of 0.05–0.6 in. H_2O/ft, with the low values used to keep the reboiler temperature low while running a moderate condenser pressure and temperature.
4. Calculate the ratio of liquid loading to vapor loading, L_f/G_f, for the column from Eqs. 4 and 5. Notice that the value of F_{pd} cancels out.
5. Using Figure 1 at the ΔP selected in Step 3, find the value of L_f/G_f calculated in Step 4 and read the corresponding value of G_f. An alternative method can be used with a computer routine when the ΔP can be calculated for various values of G_f, given L_f/G_f, until the desired ΔP is found using Eq. 3 — as long as L_f does not exceed 20,000. Eq. 3 only applies to L_f below 20,000. Use Figure 1 at higher L_f.
6. Select a packing to be used in the tower, and determine the packing factor from either Table 1, 2 or 3.
7. Calculate gas loading, in lb/hr/ft^2, $G = G_f/(0.075/\rho_g)^{0.5}(F_{pd}/20)^{0.5}$
8. Calculate the tower cross sectional area, ft^2, $A = GA/G$
9. Calculate the tower diameter, ft, $D = [4A/p]^{0.5}$
10. Check that the tower diameter is at least 8 times the packing size selected in Step 6. If not, select a smaller packing, and repeat Steps 6 through 10.

NOMENCLATURE

A= tower cross-sectional area, ft^2;
C_0= constant specific to a particular packing;
C_1= constant specific to a particular packing;
$C_3 = 7.4 \times 10^{-8}$;
$C_4 = 2.7 \times 10^{-5}$;
D= tower diameter, ft;
F_p= packing factor, dimensionless;
F_{pd}= dry-bed packing factor, dimensionless;
$F_s = V_s \rho_g^{0.5}$, ft/sec (lb/ft^3)$^{0.5}$;
G= gas loading, lb/hr-ft^2;
GA= design vapor flow rate, lb/hr;
G_f= gas loading factor;
L= liquid loading, lb/hr-ft^2;
L_f= liquid loading factor;
ΔP = specific pressure drop, in. H_2O/ft of packing;
ΔP_{pb}= specific pressure drop through dry bed, in. H_2O/ft of packing;
V_s= superficial gas velocity, ft/s;
ρ_g= gas density, lb/ft^3;
ρ_L= liquid density, lb/ft^3;
μ= liquid viscosity, centipoise;

LITERATURE CITED

1. Eckert, J. S., "Handbook of Separation Techniques for Chemical Engineers," P. A. Schweitzer, Ed., McGraw-Hill, New York (1979).
2. Strigle, R. F., Jr., "Random Packings and Packed Towers," Gulf Publishing, Houston (1987).
3. "Bulletin DC–11," Norton Co., Akron, OH (1977).
4. "Bulletin No. 217," 3rd Ed., Glitsch, Inc., Dallas (1975).
5. Leva, M., *Chem. Eng. Progress Symp. Ser.*, 50, p. 51 (1954).
6. Kister, H. Z., and D. R. Gill, "Predict Flood Point and Pressure Drop for Modern Random Packings," *Chem. Eng. Progress*, 87, (2), p. 32 (February 1991).
7. Strigle, R. F. Jr., "Packed Distillation Column Design," *Chem. Eng. Progress*, 75, p. 86 (March 1979).
8. "Bulletin MI-80," Norton Co., Akron, OH (1977).
9. "Bulletin HY-40," Norton Co., Akron, OH (1978).
10. "Bulletin NR-2," Nutter Engineering, Tulsa, OK (1988).
11. "Datasheet GR-205," Rev. 1, Norton Co., Akron, OH (1973).
12. "Datasheet GR-267A," Norton Co., Akron, OH (1968).
13. McNulty, K. J., and C. L. Hsieh, "Hydraulic Performance and Efficiency of Koch Flexipac Structured Packings," presented at the AIChE Annual Meeting, Los Angeles (1982).
14. "Datasheet TP-111," Koch Engineering Co., Wichita, KS (1962).
15. "Datasheet TP-112," Koch Engineering Co., Wichita, KS (1962).
16. "Bulletin KS-1," Koch Engineering Co, Wichita, KS (undated).
17. "Bulletin No. 520A," Glitsch, Inc., Dallas (1981).
18. "Datasheet 4-07-82," Glitsch, Inc., Dallas (1982).
19. "Bulletin No. 703," Chem-Pro Equipment Co., Fairfield, NJ (1977) [Note: now supplied by Nutter Engineering, Tulsa, OK.]
20. "Bulletin HV-610," Chem-Pro Equipment Co., Fairfield, NJ (undated) [Note: now supplied by Nutter Engineering, Tulsa, OK.]
21. "Bulletin HV-510," Chem-Pro Equipment Co., Fairfield, NJ (undated) [Note: now supplied by Nutter Engineering, Tulsa, OK.]
22. "Bulletin No. 23," Scientific Development Co., State College, PA (undated).
23. "Tri-Packs High Performance Packings Bulletin," Jaeger Products, Inc., Fountain Valley, CA (undated).
24. "Bulletin 345," Glitsch, Inc., Dallas (1986).
25. Leva, M., "Distillation with a New Plastic Dumped Packing," presented at the AIChE National Meeting, Cleveland (1982).
26. "Chemical Engineer's Handbook," 5th Ed., R. H. Perry and C. H. Chilton, Eds., McGraw-Hill, New York (1973).

46